Comparison of 30-Day Integrations with and without Cloud–Radiation Interaction

C. T. GORDON

Geophysical Fluid Dynamics Laboratory/NOAA, Princeton University, Princeton, New Jersey

(Manuscript received 2 January 1991, in final form 22 October 1991)

ABSTRACT

A parameterization package for cloud–radiation interaction is incorporated into a spectral general circulation model (GCM). Fractional cloud amount is predicted quasi-empirically; cloud optical depth is specified for warm clouds and anvil cirrus, but depends on temperature for other subfreezing clouds; the long- and shortwave cloud optical properties are linked to the cloud optical depth. The model's time-mean clouds and its radiative, thermal, and dynamical response to cloud–radiation interaction are investigated for the extended forecast range, primarily by performing two sets of 30-day integrations from real initial conditions for three Northern Hemisphere (NH) winter and three NH summer cases: (i) CLDRADI, with cloud–radiation interaction; and (ii) LONDON, with this GCM's traditional specification of climatological zonal-mean cloud amount and global-mean cloud optical properties.

The 30-day mean CLDRADI fields of total and high cloud amount and corresponding outgoing longwave radiation (OLR) fields are plausible in many respects, especially in the tropics, where the latter exhibit South Pacific convergence zone (SPCZ)-like and some intertropical convergence zone (ITCZ)-like features, in qualitative agreement with *Nimbus-7* and Earth Radiation Budget Experiment (ERBE) observations. Also, the predicted monthly mean OLR anomalies (relative to model climatology) respond to interannual variations in sea surface temperature. Cloud amount and cloud optical depth are apparently underestimated, however, over the higher-latitude oceans, especially over the Southern Hemisphere (SH) circumpolar low pressure belt and Antarctica. The zonal mean bias in shortwave and net radiation remains large at high latitudes in the summer hemisphere, despite the improved longitudinal structure in the tropics.

Cloud–radiation interaction elicits a cirrus warming response, which reduces the tropical upper-tropospheric cold bias by ~1–2 K. Over Antarctica, the warm bias in SH summer and cold bias in SH winter are both considerably reduced. During NH winter, the tropical upper troposphere experiences a significant westerly acceleration, including a sign reversal of the zonal-mean zonal wind. By being more conducive to meridional propagation, CLDRADI's tropical westerlies may contribute to the amplification of the quasi-stationary planetary waves in the SH summer extratropics. Otherwise, the impact of cloud–radiation interaction on extratropical geopotential height is generally minimal at extended range.

1. Introduction

During the 1980s, climate modelers became increasingly aware that the simulation of climate by general circulation models (GCMs) and their climate's sensitivity is affected by the treatment of cloud amount and cloud radiative properties. For example, in Shukla and Sud (1981) cloud–radiation feedback influenced the regional characteristics of their model's general circulation and the intensity of its energy cycle. Ramanathan et al. (1983) obtained favorable zonal-mean thermal and dynamical responses in their GCM's upper troposphere when they permitted high clouds to penetrate higher and to be nonblack in the infrared. Also, the GCM radiative cooling rates of Randall et al. (1989) were quite sensitive to modifications in their parameterization of cirrus clouds. Simulations of cloudiness and the earth radiation budget by climate GCMs have been discussed by Harshvardhan et al. (1989), Slingo et al. (1989), and others. Herman et al. (1980) have compared their model's radiative responses to cloud solar and longwave radiative forcing, while Slingo and Slingo (1988) have investigated their model's radiative, latent heating, thermal, and dynamical responses to cloud longwave radiative forcing.

Not surprisingly, most climate GCMs have switched from using fixed zonal-mean clouds to predicted cloud amount in their radiative transfer calculations. Similarly, many centers for numerical weather prediction (NWP) have been incorporating cloud-prediction schemes into their models, as part of an ongoing effort to improve medium- and extended-range weather forecasting skill. But the assessment of cloud parameterizations has probably received less attention for the extended range than for the climate range. One of the simplest schemes for predicting cloud amount is the venerable threshold relative humidity scheme employed by Wetherald and Manabe (1980). Though their instantaneous cloud amount is either 0% or 100%, time averaging can produce a full range of in-

Corresponding author address: Dr. C. T. Gordon, NOAA/ERL, Princeton University, Forrestal Campus, Route 1, P.O. Box 308, Princeton, NJ 08542.

termediate values. The cloud-prediction schemes employed by Shukla and Sud (1981) and by Ramanathan et al. (1983) are essentially threshold schemes as well. Unfortunately, biases in a GCM's water vapor and relative humidity fields may adversely affect the predicted cloud amount fields. Tiedke et al. (1988) reduced this bias in the tropical lower troposphere of the European Centre for Medium-Range Weather Forecasts (ECMWF) GCM by parameterizing shallow convection. Slingo (1987) partially circumvented it by developing an empirical, multipredictor cloud-prediction scheme. Relative humidity is still her primary predictor, while auxiliary predictors, that is, vertical motion, static stability, and convective precipitation, tend to be synoptic-situation specific and hence cloud-type specific. Her scheme's ability to predict fractional cloud amount is obviously desirable for forecasting applications.

Cloud optical properties are still specified as global- or zonal-mean values in some GCMs. But increasingly, they are being parameterized in terms of cloud-water path and zenith angle, as proposed by Stephens (1978), or cloud optical depth and zenith angle, as proposed by Platt and Harshvardhan (1988). In turn, the cloud-water content or path itself must be predicted, parameterized, or specified. For example, Smith (1990) and Zheng and Liou (1986) calculate the liquid water temperature and the total water content. The cloud water and cloud fraction of nonconvective clouds are diagnosed in terms of those variables. Smith (1990) takes account of quasi-Gaussian turbulent fluctuations of cloud water about their mean; his fractional cloud amount may be expressed as a function of mean relative humidity whose threshold value is related to the standard deviation of the fluctuations. A modified version of the Sundquist (1978) parameterization controls the rate at which condensed stratiform cloud water is converted into precipitation. A nice feature of Smith's approach is that it attempts to unify the physical description of clouds used to calculate precipitation, radiation, and cloudy-air turbulence.

Until now, the Experimental Prediction Group at the Geophysical Fluid Dynamics Laboratory (GFDL) has specified climatological *zonal-mean* cloud amount based upon Telegadas and London (1954) and Sasamori et al. (1972) and global-mean cloud optical properties based upon London (1957) in their global GCMs. These models have been used extensively in 30-day forecast experiments. As discussed by Miyakoda et al. (1986), systematic error becomes a dominant source of forecast error over the extended (e.g., days 10–30) range, and thus easier to detect, while the current level of forecast skill beyond 10 days is rather marginal. Of course, it affects longer-term integrations of atmospheric models with specified boundary forcing or ocean–atmosphere-coupled models. The model's systematic error has already been reduced to some extent by refining its spatial resolution, improving its subgrid-scale parameterization of turbulence, and incorporating gravity-wave drag.

Motivated by the desire to further reduce our GCM's systematic error and improve its extended-range (and ultimately even seasonal-range) forecast capability, we recently developed a parameterization package for cloud amount and cloud optical properties used in the radiative transfer calculations. Then, we carried out comparative 30-day integrations from six sets of real initial conditions to test their impact at extended range. Cloud amount and earth radiation budget verification data derived from satellite observations were obtained for selected cases, along with analyses of conventional meteorological data for all six cases. Also, we have briefly analyzed the radiative output from some recent longer-term integrations of a model similar to CLDRADI. The present paper documents the new cloud-parameterization package, examines the model's extended-range time-mean cloud prediction, and examines its corresponding radiative, thermal, and dynamical responses.

The attributes of the basic GCM are reviewed in section 2, while the parameterizations for cloud amount and cloud optical depth are documented in section 3. The control run, the basic experimental run, and various auxiliary runs are defined in terms of their respective distinguishing model characteristics; the cases and the verification datasets are briefly described in section 4. The GCM's 30-day mean predicted cloud amount fields and cloud optical properties are presented in section 5. Its time-mean radiative response to the cloud parameterizations as well as to anomalous surface boundary forcing are discussed in section 6. Temperature and zonal wind responses are described in sections 7 and 8, respectively. The geopotential height response, especially the amplification of SH summer extratropical quasi-stationary planetary waves, is the focus of section 9. Results are summarized in section 10.

2. GCM characteristics

An R21L18-resolution global spectral model is mainly used in this study. Here, R21 denotes rhomboidal truncation at wavenumber 21 and L18 denotes 18 sigma levels in the vertical, 5 of which normally reside in the boundary layer. An earlier, R21L9 version of the model was described by Gordon and Stern (1982) and used by Gordon et al. (1985) to generate satellite-derived effective low and high cloud amount fields. We opted for relatively fine vertical resolution, reasoning that the vertical placement of the clouds, especially in the upper troposphere and in the atmospheric boundary layer, would be important for validation purposes in the future, if not now. Though modest, the current R21 horizontal resolution is somewhat finer than R15, which has been frequently utilized in GCM climate simulations and sensitivity studies.

Most of the GFDL parameterizations of subgrid-scale physical processes found in the Gordon and Stern (1982) model have been retained, including vertical turbulent mixing in the planetary boundary layer and free atmosphere by the Mellor–Yamada turbulence closure scheme for unsaturated air, and in the surface boundary layer by the Monin–Obukhov formulation (Miyakoda and Sirutis 1977); ∇^4 horizontal diffusion; water-bucket hydrology; moist convective adjustment; large-scale condensation; a surface heat-balance calculation over land and sea ice; and radiation.

The radiation calculation employs the Fels and Schwarzkopf (1975) simplified exchange method for water vapor infrared cooling; Fels and Schwarzkopf (1981) CO_2 transmission coefficients; a Bignell (1970) water vapor continuum; the Lacis and Hansen (1974) ozone and water vapor absorption; and multiple reflection between clouds and the surface. The solar radiation is seasonally varying. Though diurnal variation is an option, it is currently switched off. As reported by Schwarzkopf and Fels (1991), clear-sky longwave-cooling profiles generated by the radiation code, for five standard temperature and humidity profiles adapted from McClatchey et al. (1972), compare favorably with line-by-line calculations. Clouds are either specified from the traditional climatology (see section 1) or else diagnosed from the newly implemented parameterizations for cloud amount and cloud optical properties (see section 3).

The land surface albedo and the treatment of surface albedo over snow-covered land have been revised from Gordon and Stern (1982). As described in Gordon (1986), snow albedo is a function of the albedos for fresh, deep snow; snow-free land; land surface type; and surface temperature. The latter variable is a surrogate for snowmelt, following Robock (1980). The land surface type and the albedos for fresh, deep snow and snow-free land were obtained from CLIMAP (climate: long-range investigation, mapping, and prediction) data.

Observed, seasonally varying sea surface temperatures are specified. Last, the basic model utilizes the mountain gravity-wave-drag scheme of Stern and Pierrehumbert (1988). It redistributes all of the base momentum flux within the vertical column above the base level.

3. The package of parameterizations for cloud–radiation interaction

There are three components of the parameterization package: (i) the computation of cloud amount; (ii) the treatment of cloud optical depth; and (iii) the linkage of shortwave and longwave cloud optical properties to the cloud optical depth. Fractional cloud amount is diagnosed using a modified version of the empirically based scheme of Slingo (1987). Optical depths of subfreezing low or middle clouds and nonprecipitating high clouds vary with temperature, as in Platt and Harshvardhan (1988); optical depths of other high, middle, and low clouds are fixed. The short- and longwave cloud optical properties have been made more consistent by linking them to the cloud optical depth. For this purpose, we adapted a computer code from V. Ramaswamy (personal communication, 1987).

The modified GCM possesses a *cloud–radiation interaction* capability in the sense that variations in predicted cloud amount and optical depth can directly affect the radiation field, and in turn, the thermodynamical and dynamical fields. Moreover, the predicted clouds depend on the thermodynamics and/or dynamics, but cloud water is not yet a prognostic variable.

a. Cloud amount

Our scheme closely resembles the empirically based threshold scheme of Slingo (1987). As for differences: (i) high, middle, and low cloud amount vary linearly, instead of quadratically, with relative humidity RH over the range $RH_c \leqslant RH \leqslant 1$, where RH_c is the threshold relative humidity; (ii) RH_c is reduced from 0.80 to 0.70; (iii) anvil cirrus are treated the same as other high clouds in terms of cloud amount, but have different cloud optical properties; (iv) predictor variables for layered cloud amount are time averaged between radiation time steps; (v) low clouds can be more than one sigma layer thick; (vi) shallow convective cloud amount is computed, even in the model version, which lacks a shallow-convection parameterization for water vapor transport.

Modification (i) is a somewhat ad hoc simplification, while (ii) yields a better fit to the observed global-mean cloud cover. The threshold relative humidity is less than in most other GCMs. The optimal value may be height dependent (Xu and Krueger 1991) as well as GCM dependent. Modification (iii) was made assuming that moist convective adjustment moistens the GCM's upper tropical troposphere more effectively than the Kuo scheme did in the ECMWF model studied by Slingo (1987). Modification (iv) was implemented to control noise, but had little effect on stratiform clouds in practice. Modification (v) recognizes that some low-cloud systems, such as those associated with synoptic disturbances, are thicker than others, such as marine stratocumulus. Modification (vi) is a crude attempt to represent trade wind cumulus clouds.

The basic cloud-prediction scheme treats five cloud types: high-, middle-, and low-layer clouds, convective clouds (cf. Slingo 1987), and trade-wind cumulus or shallow convective clouds. The distinction between low, middle, and high σ levels for layer clouds is specified a priori. The low–middle and middle–high boundaries vary with latitude and season in a similar manner as the specified climatological zonal-mean cloud tops and bases (see Fig. 1 of Gordon et al. 1985). A preliminary calculation of cloud amount, that is, the

fraction of the grid box containing cloud, is made at each level beneath the top level ($\sigma = 0.009$), including the lowest level ($\sigma = 0.998$).

These cloud amounts are diagnosed by a set of 13 equations, which are documented below for completeness. Apart from the differences highlighted in the preceding, however, the equations resemble the empirically based formulas of Slingo (1987) in form, and, unless otherwise noted, the values of the empirical constants are the same.

High cloud amount n_h is given by

$$n_h = \begin{cases} 0.0 \\ (\mathrm{RH} - \mathrm{RH}_c)(1.00 - \mathrm{RH}_c)^{-1}, \\ 1.0 \end{cases} \quad \text{if} \quad \begin{cases} \mathrm{RH} < \mathrm{RH}_c \\ \mathrm{RH}_c \leqslant \mathrm{RH} \leqslant 1.0, \\ \mathrm{RH} > 1.0 \end{cases} \tag{1}$$

where RH is the relative humidity and RH_c is the threshold value, 0.70.

Similarly, middle cloud amount n_m is given by

$$n_m = \begin{cases} 0.0 \\ (\mathrm{RH}_e - \mathrm{RH}_c)(1.00 - \mathrm{RH}_c)^{-1}, \\ 1.0 \end{cases} \quad \text{if} \quad \begin{cases} \mathrm{RH}_e < \mathrm{RH}_c \\ \mathrm{RH}_c \leqslant \mathrm{RH}_e \leqslant 1.0, \\ \mathrm{RH}_e > 1.0 \end{cases} \tag{2}$$

where RH_e is the relative humidity after adjustment for the convective cloud amount n_{cnv}, that is,

$$\mathrm{RH}_e = \mathrm{RH}(1.00 - n_{\mathrm{cnv}}). \tag{3}$$

Low stratiform clouds fall into two classes. Class I is associated with large-scale ascent of moist air; class II is linked to boundary-layer stratus, and is associated with a temperature inversion. For class I, the low cloud amount n_{l1} is expressed as a product of two functions, that is,

$$n_{l1} = A(\mathrm{RH}_e)B(\omega). \tag{4}$$

The function A depends on relative humidity only and B on the pressure vertical velocity ω only,

$$A(\mathrm{RH}_e) = \begin{cases} 0.0 \\ (\mathrm{RH}_e - \mathrm{RH}_c)(1.00 - \mathrm{RH}_c)^{-1}, \\ 1.0 \end{cases} \quad \text{if} \quad \begin{cases} \mathrm{RH}_e < \mathrm{RH}_c \\ \mathrm{RH}_c \leqslant \mathrm{RH}_e \leqslant 1.0, \\ \mathrm{RH}_e > 1.0 \end{cases} \tag{5}$$

$$B(\omega) = \begin{cases} 1 \\ \omega/\omega_0, \\ 0 \end{cases} \quad \text{if} \quad \begin{cases} \omega < \omega_0 \\ \omega_0 \leqslant \omega \leqslant 0.0, \\ \omega > 0.0 \end{cases} \tag{6}$$

and $\omega_0 = -3.6$ hPa h^{-1}. Low cloud amount n_{l1} is diminished by weak vertical ascent and vanishes in a subsiding environment. Similarly, for class II, the low cloud amount n_{l2} is a product of two functions:

$$n_{l2} = S\left(-\frac{\Delta\theta}{\Delta p}\right)B(\mathrm{RH}_{\mathrm{base}}), \tag{7}$$

$$S\left(-\frac{\Delta\theta}{\Delta p}\right) = \begin{cases} 1.0 \\ -6.67\,\dfrac{\Delta\theta}{\Delta p} - 0.667, \\ 0.0 \end{cases} \quad \text{if} \quad \begin{cases} \dfrac{\Delta\theta}{\Delta p} < -0.25 \\ -0.25 \leqslant \dfrac{\Delta\theta}{\Delta p} \leqslant -0.10, \\ -0.10 < \dfrac{\Delta\theta}{\Delta p} \end{cases} \tag{8}$$

$$B(\mathrm{RH}_{\mathrm{base}}) = \begin{cases} 1 \\ (\mathrm{RH}_{\mathrm{base}} - 0.6)/0.2, \\ 0 \end{cases} \quad \text{if} \quad \begin{cases} 0.8 < \mathrm{RH}_{\mathrm{base}} \\ 0.6 \leqslant \mathrm{RH}_{\mathrm{base}} \leqslant 0.8. \\ \mathrm{RH}_{\mathrm{base}} < 0.6 \end{cases} \tag{9}$$

Here, θ is the potential temperature, p is the pressure, $\Delta\theta/\Delta p$ is the lapse rate (K hPa^{-1}) in the most stable layer below 750 hPa, and $\mathrm{RH}_{\mathrm{base}}$ is the relative humidity at the base of the inversion.

Neither class of low stratiform cloud is likely to occur in the trade-wind cumulus region. Class I is inhibited by the combined effects of subsidence (or weak upward vertical motion) and excessive drying, especially above $\sigma = 0.901$. Meanwhile, the model-predicted vertical temperature profiles are nearly moist adiabatic [in contrast to those of the ECMWF model with Kuo convection but *without shallow convection* (Tiedke et al. 1988), which reveal an excessive inversion]. Thus, they are not conducive to class II low clouds. For the reasons cited, we introduce a trade-wind cumulus or shallow convective cloud amount n_{shl}:

$$n_{\mathrm{shl}} = C_{\mathrm{shl}}A(\mathrm{RH}_e). \tag{10}$$

We obtain $A(\mathrm{RH}_e)$ from Eq. (5) and $C_{\mathrm{shl}} = 0.2$. In the basic model version, Eq. (10) is evaluated at all levels below 750 hPa, which are conditionally unstable ($\partial\theta_e/\partial p \geqslant 0$, θ_e being the equivalent potential temperature) and simultaneously exhibit large-scale descent or weak vertical ascent ($\omega < \omega_0$). Although this model version lacks parameterized shallow convection, shallow convective cloud is categorized as another form of low cloud. Utilizing Eqs. (8), (9), and (10), the low cloud amount is

$$n_l = \max(n_{l1}, n_{l2}, n_{\mathrm{shl}}). \tag{11}$$

Information on cloud subtype corresponding to the solution of Eq. (11) is carried along.

After evaluating Eqs. (1)–(11) at each sigma level, high, middle, and low clouds are assigned to those three distinct sigma levels σ_h, σ_m, and σ_l in the upper, middle, and lower troposphere, respectively, where n_h, n_m, and n_l attain their maximum values; and the corresponding fractional cloud amounts are set to those maximum values:

$$\begin{bmatrix} n_h(\sigma_h) \\ n_m(\sigma_m) \\ n_l(\sigma_l) \end{bmatrix} = \max\begin{pmatrix} n_h\text{'s} \\ n_m\text{'s} \\ n_l\text{'s} \end{pmatrix}. \quad (12)$$

High, middle, and low clouds are generally one sigma layer thick in the 18-level model, though such a constraint would be less appropriate if the model's vertical resolution were refined. But even in the R21L18 model, cloud-type information is used to adjust the thickness of some clouds. In particular, in an environment with strong vertical ascent ($\omega < \omega_0$), the tops of class I low clouds are elevated one sigma level to level σ_{l-1}, if $0 < n_{l1}(\sigma_l) - n_{l1}(\sigma_{l-1}) < 0.25$. Likewise, in the basic model version, shallow convective clouds are elevated one sigma level.

Shallow convective cloud is treated differently in the newer model version with parameterized shallow convection. First, it is a distinct cloud type. Second, the cloud occupies the same layer as the shallow convection. Thus, its base is at the sigma level nearest to the lifting condensation level (LCL), while its top is at the sigma level nearest to the level of zero buoyancy, or 750 hPa, whichever is lower in the atmosphere. In practice, the lid at 750 hPa usually has to be invoked, even if a more precise formula than $\partial\theta_e/\partial p = 0$ is used to compute the buoyancy. Third, the maximum value of n_{shl} between the cloud base and top, as obtained from Eq. (10), is assigned to all levels within the cloud. Fourth, n_{shl} is excluded from Eq. (11) and does not affect Eq. (12) either. But after solving Eq. (12) and adjusting the thickness of class I low clouds, n_{shl} is finally compared to n_l at low sigma levels. Wherever $n_{\text{shl}} > n_l$, the cloud amount is changed to n_{shl} and the cloud type to shallow convective.

Meanwhile, convective cloud amount in the lower troposphere is given by

$$n_{\text{cnv}} = \begin{cases} 0.0 \\ a + b\ln P, \\ 0.8 \end{cases} \quad \text{if} \quad \begin{cases} P < 0.14 \\ 0.14 \leqslant P \leqslant 85.0, \\ 85.0 < P \end{cases} \quad (13)$$

where $b \sim 0.125$ and $a \sim -0.125\ \ln(0.14)$ are empirical constants and P is the model's convective precipitation rate in millimeters per day, averaged between radiation time steps (currently 12 h). However, for convective towers in the middle and upper troposphere, Eq. (13) is scaled by 0.25. The cloud top and base are defined by the block of contiguous sigma levels where convection has occurred (not necessarily simultaneously) between radiation time steps.

When deep convective and stratiform clouds coexist at levels σ_h, σ_m, or σ_l, then n_{cnv} is usually added to n_h, n_m, or n_l assuming random overlap. However, if the cloud type is shallow convective, that is, if $n_l = n_{\text{shl}}$, we set n_l or $n_{\text{shl}} = 0$ if $n_{\text{cnv}} \geqslant n_{\text{shl}}$, or $n_{\text{cnv}} = 0$, if $n_{\text{cnv}} < n_{\text{shl}}$. At levels σ_h, σ_m, or σ_l, the cloud type is classified as convective only if $n_{\text{cnv}} \geqslant n_h$, $n_{\text{cnv}} \geqslant n_m$, or $n_{\text{cnv}} \geqslant n_l$, respectively. Otherwise, the cloud type is high, middle, low class I, low class II, or low shallow convective. Any convective cloud that penetrates a high, middle, or low cloud layer is broken into two discrete, randomly overlapping segments, one below and one above that layer. Similarly, the convective tower (where n_{cnv} is scaled by 0.25) is currently regarded as a distinct, randomly overlapping cloud segment. This treatment is dictated by a constraint in the present radiation code, that is, different clouds in a vertical column (layered and convective alike) are assumed to randomly overlap. The cloud type of each convective segment between the cloud base and top is classified as convective. Random overlap is assumed between all distinct cloud layers and convective segments to compute the total cloud amount.

b. Parameterization of cloud optical depth

Visible optical depths of "cold" clouds ($T_c < -10°\text{C}$) other than precipitating high clouds vary quadratically with the departure of cloud mean temperature T_c from a very cold reference value T_{c0}:

$$\tau_{\text{SW}} = A(T_c - T_{c0})^2, \quad T_{c0} < T_c < -10°\text{C}, \quad (14)$$

where, $T_{c0} = -82.5$ K. Equation (14) is adapted from Harshvardhan et al. (1989), who based their formulation on the empirical results of Platt and Harshvardhan (1988). But the coefficient A incorporates a high-, middle-, or low-cloud pressure thickness Δp_c and has been further enhanced. For high clouds, for example, $\Delta p_c = 31.25$ hPa while $A = 4 \times 10^{-4}$, or roughly three times larger than their value. Even so, $\tau_{\text{SW}} < 0.5$ for many "cold," nonprecipitating high clouds.

In Harshvardhan et al. (1989), "warm" cloud ($T_c > 0°\text{C}$) optical depths are linearly proportional to the actual cloud pressure thickness Δp. However, when this parameterization was applied to our 18-level GCM, low clouds beneath $\sigma = 0.901$ tended to have smaller Δp's and hence smaller albedos than middle clouds; consequently, the planetary albedo was too low. Conversely, when we relaxed the constraint that there be no more than one low, middle, and high stratiform cloud layer, the planetary albedo increased to an unacceptably high value of 0.35. To circumvent this problem, we specify distinct visible optical depths for warm low, middle, and high stratiform clouds, precipitating high clouds, including anvil cirrus, and convective clouds. Anvil cirrus occurs if the rate of con-

vective precipitation falling from high plus middle layers beneath a "high" cloud top exceeds 0.5 mm day^{-1}. The fixed visible optical depths for warm low clouds, warm middle clouds, warm and/or precipitating high clouds, anvil cirrus, shallow convective clouds, and precipitating convective clouds are 9.0, 6.0, 2.5, 5.0, 9.0, and 18.0, respectively.

For "cool" clouds with mean temperatures in the intermediate range $-10° < T_c < 0°C$, the cloud optical depth is linearly interpolated between the values for cold clouds with $T_c = -10°C$ and warm clouds. An adjustment is made for "thin" low clouds, whether warm or cold, whose tops are below level 15 ($\sigma = 0.901$) of the 18-level GCM. Namely, their optical depths are diminished by $(1 - \sigma_{top})(1 - 0.901)^{-1}$.

c. *Shortwave and longwave cloud radiative properties*

In the past, shortwave and longwave radiative properties were specified independently in our GCM. This remains the case for the control integration with fixed clouds. However, in the new cloud–radiation interaction package, these properties are specified in a more self-consistent manner. This approach is desirable in the long term, as the GCM cloud–radiation code becomes increasingly interactive. Stephens (1978) proposed a parameterization for GCMs that links the shortwave and longwave properties through their mutual dependence on the cloud liquid water path; the approach was extended to ice clouds by Stephens and Webster (1981). We have adopted a variation of this approach, suggested by V. Ramaswamy (personal communication, 1987) that is quite convenient when cloud water is not a prognostic GCM variable. Namely, the cloud reflectivities (R_{vis} and R_{nir}) and absorptivities (A_{vis} and A_{nir}) for the visible (vis) and near-infrared (nir) spectral bands are computed as functions of the shortwave optical depth τ_{SW} and zenith angle, and the longwave emissivity ϵ_{LW} as a function of the infrared absorption optical depth τ_{LW}. Platt and Harshvardhan (1988) and Harshvardhan et al. (1989) also linked their shortwave and longwave cloud optical properties to τ_{SW}. The calculation of R_{vis}, R_{nir}, A_{vis}, and A_{nir} is based on the δ-Eddington approximation, following Joseph et al. (1976). The radiation is diffuse beneath the first cloud layer where the cumulative cloud optical depth exceeds 1. Given τ_{SW}, the liquid water fraction β, and the shortwave specific extinction K_{SWI} and K_{SWL} for ice particles and liquid cloud droplets, one can diagnose the effective cloud ice water path (IWP) and cloud liquid water path (LWP) from the equation

$$\tau_{SW} = (K_{SWI})(IWP) + (K_{SWL})(LWP). \quad (15)$$

We assume that $\beta = 0$ for $T < 258$ K (pure ice phase), $\beta = 1$ for $T > 268$ K (pure liquid phase), and β varies linearly with temperature for $258 < T < 268$ K (mixed phase). The system is closed by computing the ratio IWP/LWP and eliminating the total cloud-water path CWP from

$$LWP = \beta(CWP); \quad IWP = (1 - \beta)(CWP). \quad (16)$$

The emissivity is given by

$$\epsilon_{LW} = 1 - \exp(-b\tau_{LW}), \quad \text{where} \quad (17)$$

$$\tau_{LW} = (K_{LWI})(IWP) + (K_{LWL})(LWP), \quad (18)$$

b is the diffusivity factor ($b = 1.66$), and K_{LWI} and K_{LWL} are the longwave specific absorption for ice particles and liquid droplets. We adopted the following values: $K_{SWI} = 74$ m^2 kg^{-1}, $K_{SWL} = 130$ m^2 kg^{-1}, $K_{LWI} = 60$ (i.e., $100/b$) m^2 kg^{-1}, and $K_{LWL} = 84$ (i.e., $140/b$) m^2 kg^{-1}. We were guided by Stephens (1978) for the value of K_{LWI} and by Ramaswamy and Ramanathan (1989) for the value of K_{SWI}. However, the ratios τ_{LW}/τ_{SW} for pure ice or pure water are somewhat larger than those calculated by Platt (1983). The asymmetry parameter = 0.80, while the single-scattering albedo in the near IR is given by $\omega_0 = 0.99420$.

4. The setup

a. *The integrations*

Thirty-day comparative integrations have been performed for three Northern Hemisphere (NH) winter [Southern Hemisphere (SH) summer] cases and three NH summer cases using two model versions, hereafter referred to as *CLDRADI* and *LONDON*. CLDRADI employs the new package of parameterizations for cloud–radiation interaction described in section 3. In contrast, the control model LONDON utilizes the GCM's traditional specification of climatological zonal-mean cloud amounts and global-mean cloud absorptivities, reflectivities, and blackbody emissivities. The two GCMs are identical in all other respects and possess the features summarized in section 2.

Also, the following auxiliary integrations have been performed to help to clarify the results. *LONDON-adj*: the same as LONDON, except that longwave vertical adjustment, that is, vertical smoothing of the in-cloud longwave cooling profile, is restored. (This smoothing is switched off in CLDRADI and LONDON.) *CLDRADI-tau*: the same as CLDRADI, except that the temperature-dependent optical depth formula for cold clouds is suppressed, and fixed values for warm clouds are used instead. *CLDRADI-scg (R21L18; R42L18; or T30L18)*, where R denotes rhomboidal and T triangular spectral truncation: the same as CLDRADI plus parameterized shallow convection in the spirit of Tiedke et al. (1988) and reformulated gravity-wave drag after Pierrehumbert (1987). The latter scheme deposits momentum only at levels where wave breaking occurs, mainly above the tropospheric westerly jet maximum; and some of the base momen-

tum flux may escape to space. *RH100*: a binary cloud-prediction scheme (0% or 100% cloud amount) similar to that of Wetherald and Manabe (1980). Relative humidity is the only predictor; the threshold relative humidity is 100%, a value slightly greater than theirs; clouds are not allowed in the model's lowest two sigma layers; and their optical properties are the same as LONDON's.

RH100 was integrated for one NH winter case; and CLDRADI-tau and LONDON-adj for six cases. The R21L18 and R42L18 versions of CLDRADI-scg have recently been integrated for one summer (ISCCP) case to test the sensitivity of the predicted clouds to GCM resolution, while the T30L18 version was recently integrated in climate mode to investigate the model's response (especially during the summer drought of 1988) to anomalous surface boundary forcing. For convenience, the distinguishing characteristics of these models are summarized in Table 1.

b. *The cases*

Six cases were selected for the CLDRADI and LONDON runs—three NH winter cases and three NH summer cases. They are identified by the dates of their initial conditions: 5 January 1979, 15 December 1982, and 15 December 1986; and 11 June 1979, 10 July 1983, and 15 July 1985. The initial time is 1200 UTC. These are the same cases that modelers attending the Workshop on Systematic Errors in Models of the Atmosphere, held in Toronto in 1988, were requested to integrate [by the World Meteorological Organization Commission for Atmospheric Sciences/Joint Scientific Committee (CAS/JSC) Working Group on Numerical Experimentation, 1988] to foster model intercomparison of systematic errors. In preparation for this workshop, initial conditions were processed for the GFDL spectral model for all six cases. In addition, we had previously processed earth radiation budget verification data for two of the cases. Thus, these six cases seemed convenient for studying the model's systematic error response to the incorporation of cloud–radiation interaction. Though the sample size is quite small, the three-case winter and summer ensembles should indicate the predominant cloud–radiation-induced systematic differences, especially for zonal means.

TABLE 1. Model characteristics.

Experiment name	Description
CLDRADI	Basic model with new cloud-prediction scheme
LONDON	Basic control model with fixed zonal-mean clouds
LONDON-adj	Same as LONDON, except LW-cooling profiles are smoothed
CLDRADI-tau	Same as CLDRADI, except for optical depth of cold clouds
CLDRADI-scg R21L18 R42L18 T30L18	CLDRADI + shallow convection + modified gravity-wave drag at the designated spectral and vertical resolution
RH100	With Wetherald–Manabe type of cloud-prediction scheme

Hereafter, if no ambiguity arises, the NH winter cases and NH summer cases will be referred to as *winter cases* and *summer cases,* respectively. However, when focusing on the Southern Hemisphere, we may refer, more explicitly, to SH summer or SH winter cases.

c. *Verification data and initial conditions*

Verification data for clouds and radiation were obtained from several sources. Monthly mean *Nimbus-7* narrow-field-of-view (NFOV) broadband earth radiation budget (ERB) data at the top of the atmosphere (TOA) were processed for January, June, and July of 1979, while corresponding deconvolved wide-field-of-view (WFOV) ERB data were processed for January 1983. Following Slingo et al. (1989), the systematic bias of the *Nimbus-7* NFOV ERB fluxes was essentially removed by adding 3 W m^{-2} to the outgoing longwave radiation (OLR) and reducing the planetary albedo by 9% of its original value. For January 1979, we assumed that the monthly mean day–night longwave flux differences were the same as for January 1980, since the nighttime fluxes were not available. The above *Nimbus-7* ERB data together with global temperature and water vapor analyses were input into our GCM to derive monthly mean high and low (and total) "effective" cloud amount fields for January, June, and July 1979 and January 1983, using the technique of Gordon et al. (1985). These "NIMCLD" effective clouds were originally generated due to the unavailability of satellite-derived "observed" global cloud data. They may be thought of as a radiatively constrained, two-layer approximation to the observed cloud distribution, except at high latitudes, where weak (if any) solar insolation and/or significant snow cover are found in conjunction with a low-level temperature inversion. Also, we have processed June 1979 and July 1979 monthly mean cloud amount fields from the NESDIS (National Environmental Satellite Data Information Service) multiyear *Nimbus-7* C-matrix dataset (Stowe et al. 1989), hereafter referred to as STOWE; and more recently, July 1985 monthly mean ERBE (Earth Radiation Budget Experiment) NFOV scanner data (Barkstrom et al. 1990). Last, we have obtained STOWE and ISCCP (International Satellite Cloud Climatology Project) (Rossow et al. 1989, 1990), zonal-mean, monthly mean cloud data for July 1983.

Verification data and initial conditions for dynamical and thermodynamical variables were derived from National Meteorological Center (NMC) analyses for all six cases. Compared to the cloud and ERB data, this data is better synchronized in time with our model's output.

d. Verification strategy

For dynamical and thermodynamical variables, 20-day means are generally computed to minimize spinup effects. In contrast, for model-predicted clouds or earth radiation budget data, we focus on 30-day mean predictions to facilitate comparison with monthly mean verification data. The latter comparisons will be restricted essentially to individual cases. This strategy was originally dictated by the lack of verification data for some cases. Moreover, the intercase diversity of sources of verification data, coupled with uncertainty as to the true observed state, especially for clouds, could introduce some artificial intercase variability into the observations. Even for a particular case, factors such as unrepresentative temporal satellite sampling or the lack of perfect synchronization between the forecast period and the verification period could contribute to apparent differences between forecast and observation. It is hoped that the verification of the gross, large-scale structures will still be meaningful. However, the analysis of the aforementioned factors is beyond the scope of the present study.

5. CLDRADI simulation of cloud optical properties and cloud amount

Cloud optical properties were calculated off-line for representative values of shortwave optical depth. The results are summarized in Table 2, along with the LONDON cloud optical properties. The GCM-predicted high clouds are slightly less emissive ($\epsilon_{LW} = 0.96$ vs 1.00) and somewhat more reflective ($R_{vis} = 0.27$ vs 0.21) than the LONDON high clouds. Also, CLDRADI clouds absorb more near-infrared radiation than LONDON through most of the troposphere. Figure 1 depicts the CLDRADI 30-day winter ensemble mean zonal-mean cloud emissivity, nir reflectivity, and nir absorptivity in the latitude–σ plane. The plotted values were computed off-line, assuming overcast conditions, wherever and whenever cloud was present, from the values diagnosed by the model's radiation code at every model grid point and radiation time step. Above 300 hPa, the zonal-mean emissivity is less than 0.8, even in the tropics, due to the presence of optically thin cirrus. However, values of $\epsilon_{LW} > 0.95$ are quite common, locally, in active regions of the tropics. The maximum zonal-mean CLDRADI reflectivities for low clouds are 0.551 and 0.506, respectively, in the vis and in the nir (not shown) bands. In contrast, according to Table 2, the LONDON low cloud reflectivities are fixed at 0.59 in both spectral bands. The maximum CLDRADI zonal mean nir absorptivity ($\sim$0.10) is larger than the fixed value (0.04) for LONDON low clouds. The CLDRADI reflectivity and absorptivity decrease at high latitudes, consistent with the temperature-dependent cloud optical depths; they also decrease near the surface, consistent with the optical depth scaling for "thin" low clouds.

TABLE 2. Cloud optical properties.

Cloud type	Phase	τ_{SW}	R_{vis}	R_{nir}	A_{nir}	ϵ_{LW}
LONDON clouds						
High	—	—	0.210	0.210	0.005	1.000
Middle			0.450	0.450	0.020	1.000
Low			0.590	0.590	0.035	1.000
CLDRADI clouds (calculated off-line for specified τ_{SW} and phase)						
Thin cirrus	Ice	0.50	0.070	0.056	0.005	0.491
High	Ice	2.50	0.273	0.226	0.023	0.966
Middle	Water	6.00	0.474	0.351	0.044	0.998
Low	Water	9.00	0.574	0.438	0.065	1.000
Deep convection	Ice*	18.00	0.730	0.605	0.148	1.000

* Cloud top is much above the freezing level.

Thirty-day mean, zonal-mean cloud amount is plotted versus latitude and σ in Fig. 2 for CLDRADI and the auxiliary RH100 run. The comparison is for a single winter case, 5 January 1979, although the CLDRADI results are representative of the three-case ensemble mean. As noted earlier, RH100 is quite similar to the cloud prediction scheme of Wetherald and Manabe (1980), which has been employed for many years in the GFDL climate model. Meanwhile, CLDRADI may be thought of as a modified version of the RH100 threshold scheme, with some bells and whistles. Thus, the sensitivity of the predicted clouds in our GCM to those bells and whistles is of some interest. CLDRADI generates more *middle* cloudiness, but less low cloudiness than RH100. The former result reflects *a sensitivity to the 30% CLDRADI–RH100 difference in threshold relative humidity,* which is enhanced by the model's midtropospheric dryness. On the other hand, the vertical motion factor in Eq. (4) tends to inhibit the formation of *low* cloud in CLDRADI. At high latitudes, CLDRADI's distinct middle and high cloud layers may be influenced by the scheme's restrictions on the number of low, middle, and high cloud layers and their vertical placement. In RH100, low clouds tend to form at the lowest permitted level of the 18-level GCM, $\sigma_{16} = 0.947$, irrespective of latitude. CLDRADI low clouds are permitted at the lowest σ level, $\sigma_{18} = 0.998$, but form over a range of σ levels. The structure of the RH100 cross section in Fig. 2 was essentially preserved when the threshold humidity was reduced to 95%, although the global-mean total cloud amount increased substantially from 0.441 (Table 3) to 0.626. The main effect of shallow convection (not shown) was to elevate CLDRADI's low cloud tops to $\sigma = 0.777$ at subtropical and tropical latitudes.

Latitudinal profiles of CLDRADI and LONDON 30-day time-mean, zonal-mean *total* cloud amount for the 10 July 1983 case are compared with July 1983 monthly mean ISCCP and STOWE "observations" in Fig. 3. (The latter two curves were replotted from Fig.

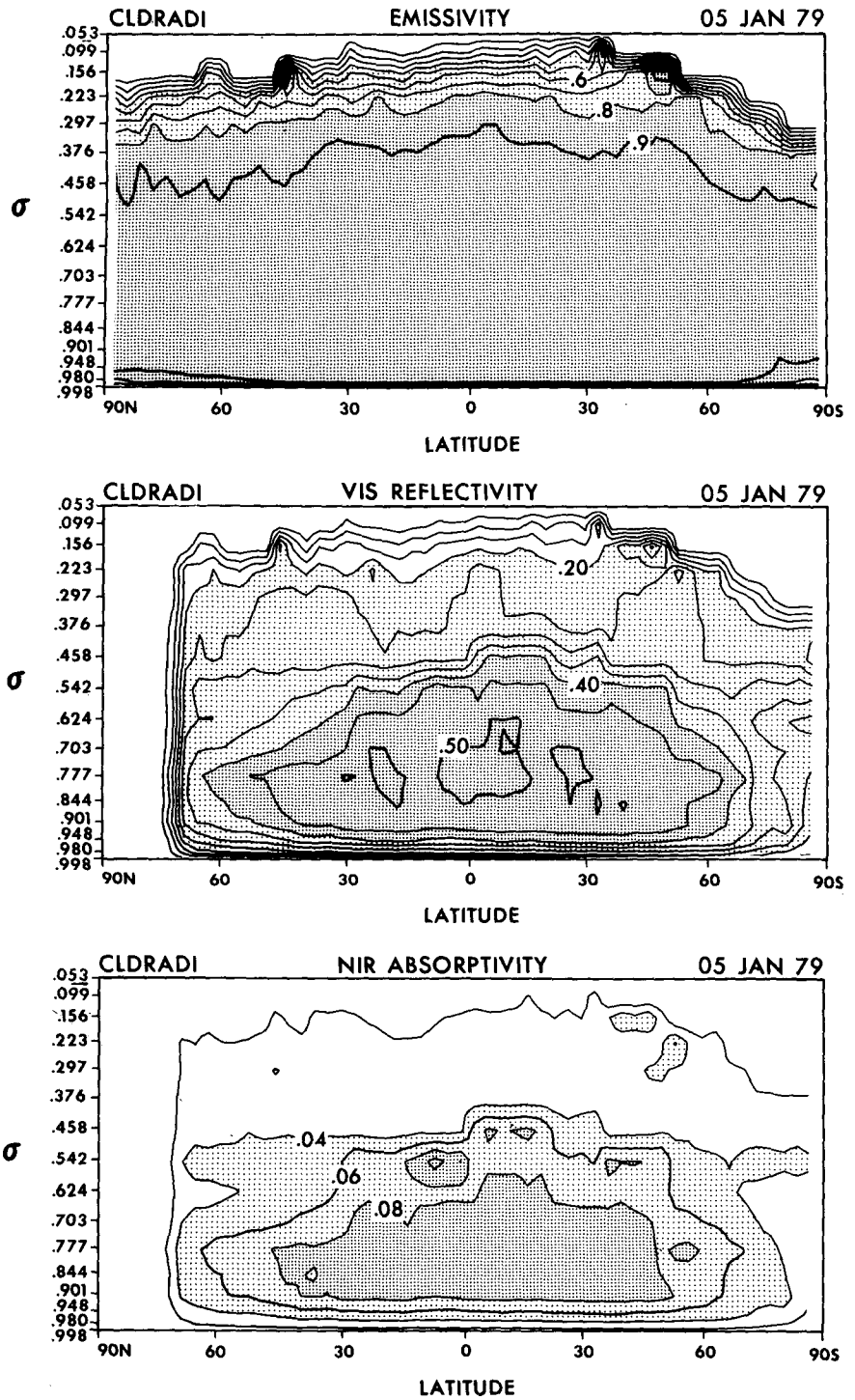

FIG. 1. Thirty-day (days 0–30) winter ensemble-mean, zonal-mean cloud optical properties. Cloud emissivity (top); vis reflectivity (middle); nir absorptivity (bottom). Contour interval = 0.1 (top); 0.05 (middle); 0.02 (bottom).

15 of Stowe et al. 1989.) CLDRADI exhibits considerably more zonal-mean cloudiness than LONDON in the tropics, the only region where CLDRADI clearly verifies better against observation. North of 40°S, CLDRADI lies between ISCCP and STOWE, but tends to agree more with STOWE, except between 10° and 25°N and north of 50°N. According to Rossow (personal communication, 1990), the threshold for de-

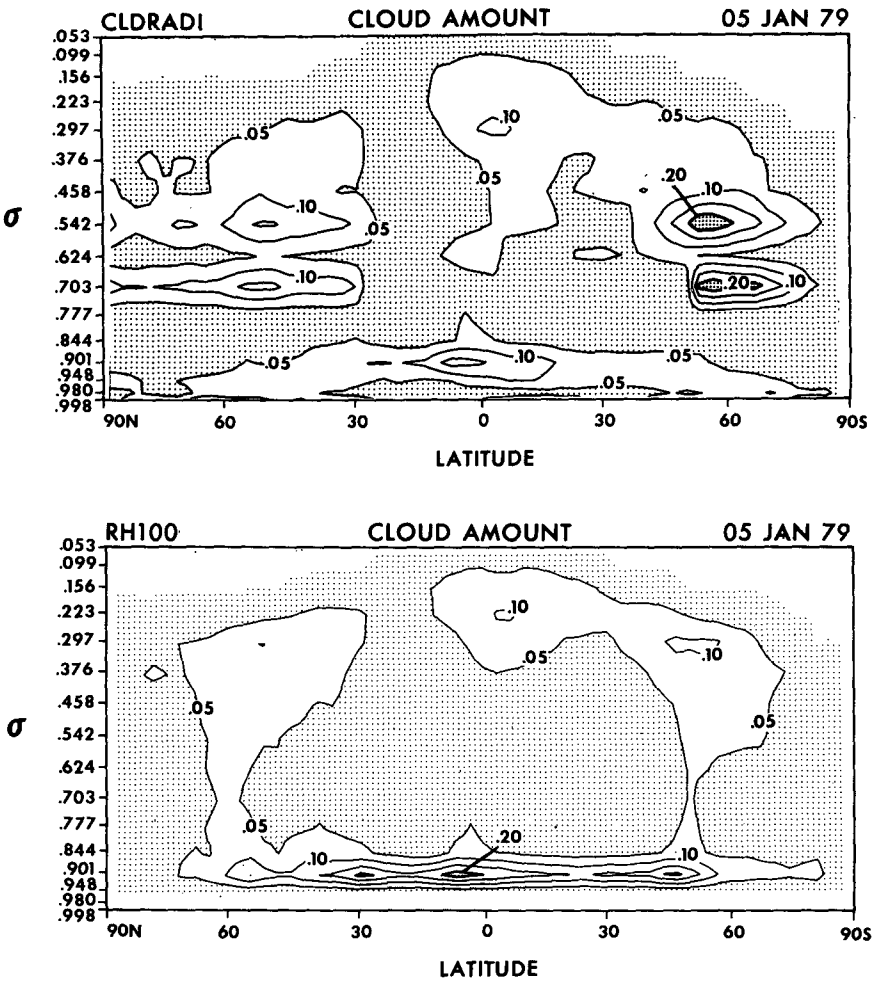

FIG. 2. Thirty-day (days 0–30) mean, zonal-mean total cloud amount for the 5 January 1979 case. CLDRADI (top); RH100 (bottom). Contour interval = 0.05. Stippling: <0.05, coarse; >0.20, fine.

tecting low clouds accounts for much of the discrepancy between ISCCP and STOWE. CLDRADI grossly underpredicts cloudiness over Antarctica.

Figure 4 shows the sensitivity of the CLDRADI results in Fig. 3 to model resolution (cf. CLDRADI-scg R21L18 vs CLDRADI-scg R42L18) and to revised physics (cf. CLDRADI-scg R21L18 vs CLDRADI). Recall that CLDRADI-scg has the same physics as

TABLE 3. Hemispheric and global-mean total cloud amount.

Dataset	NH mean	SH mean	Global mean
D0030[a] 5 January 1979 CLDRADI	0.523	0.561	0.542
Winter climatology LONDON	0.488	0.520	0.504
January 1979 MM[b] NIMCLD	0.583	0.502	0.542
D0030 5 January 1979 RH100	0.439	0.443	0.441
D0030 5 January 1979 RH95[c]	0.617	0.635	0.626
D0030 11 June 1979 CLDRADI	0.556	0.488	0.522
Summer climatology LONDON	0.521	0.486	0.503
June 1979 MM NIMCLD	0.596	0.605	0.601
June 1979 MM STOWE	0.552	0.532	0.542

[a] D0030 = 30-day mean from day 0 to 30.
[b] MM = monthly mean.
[c] Same as RH100, except threshold relative humidity is reduced to 95%.

CLDRADI, plus parameterized shallow convection and reformulated gravity-wave drag. Total (as well as low and middle) cloud amount *increases* moderately with resolution near the SH circumpolar low pressure belt and more drastically at polar latitudes, especially in the SH. This response is probably linked to the spectral truncation of water vapor, which can produce large changes in relative humidity (the primary cloud predictor) in cold, high-latitude regions, particularly in *coarser*-resolution models. The R42 model produced a modest decrease (~4%) in high cloud amount (not shown) relative to the R21, while the global mean total cloud cover did not change. In contrast, Kiehl and Williamson (1990) reported a drastic decrease in total cloud cover in the National Center for Atmospheric Research (NCAR) Community Climate Model as its resolution was refined from R15 to T63.

In the subtropical subsidence belt, total (as well as middle and high) cloud amount displays moderate sensitivity to the revised physics. There, shallow convection could conceivably reduce the cloud amount, by evicting water vapor from the boundary layer and transporting it away from the subtropics. Likewise, changes in the zonal and meridional circulations, associated with the reformulated gravity-wave drag, might affect the water vapor flux. But a detailed analysis of the physical mechanisms involved is beyond the scope of this study.

Referring to Table 3, CLDRADI's global-mean total cloud amount (0.542 in winter and 0.522 in summer) agrees quite well with NIMCLD in NH winter and STOWE in NH summer, but is ~8% lower than ISCCP (not shown). CLDRADI's global means are 2%–4% higher than LONDON.

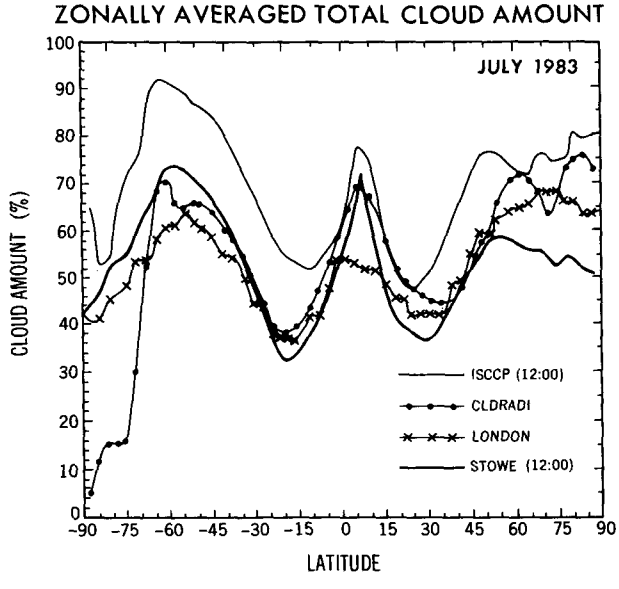

FIG. 3. Zonal-mean total cloud amount vs latitude. CLDRADI 30-day (days 0–30) mean for the 10 July 1983 case; LONDON summer climatology; ISCCP and STOWE (labeled *Nimbus-7* in Fig. 15 of Stowe et al. 1989) July 1983 monthly mean observations.

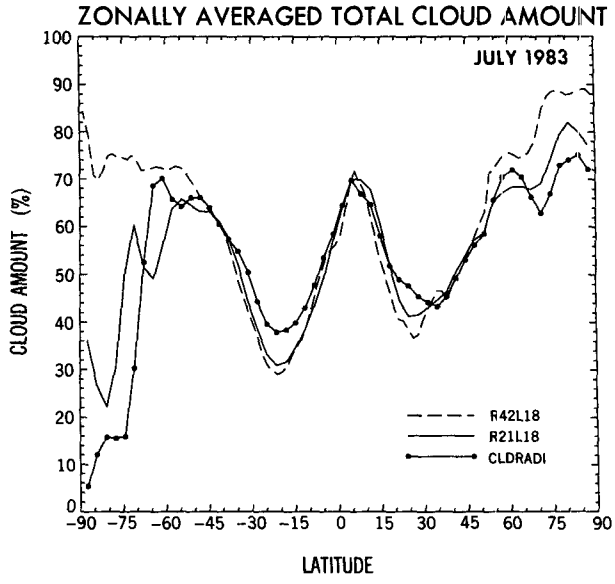

FIG. 4. Zonal-mean total cloud amount vs latitude. CLDRADI, CLDRADI-scg R21L18, and CLDRADI-scg R42L18 30-day (days 0–30) means for the 10 July 1983 case.

Thirty-day mean (days 0–30) CLDRADI *total* cloud amount fields are verified for one winter case (5 January 1979) and one summer case (11 June 1979) in Figs. 5 and 6, respectively. The corresponding NIMCLD and RH100 January 1979 monthly mean fields are included in Fig. 5 and the June 1979 monthly mean STOWE and NIMCLD fields in Fig. 6.

In the 5 January 1979 case, the structure of the CLDRADI and RH100 total cloud amount fields are in qualitative agreement, especially over the ITCZ (intertropical convergence zone) and SPCZ (South Pacific convergence zone) and over the North Atlantic and North Pacific. But CLDRADI exhibits systematically more cloud cover than RH100. Like NIMCLD, CLDRADI and RH100 display recognizable SPCZs. Over the Amazon, the predicted maxima are considerably weaker than NIMCLDs. Possible causes are horizontal resolution, surface hydrology, convective parameterization, and lack of diurnal variation. The NIMCLD feature in the southern Atlantic convergence zone is not well simulated by either prediction. Off the west coasts of South America and southern Africa, CLDRADI predicts somewhat more cloud than RH100.

In the 11 June 1979 case (Fig. 6), fairly good qualitative agreement between CLDRADI and STOWE total cloud amount is found in the tropics and subtropics, and over the North Pacific and North Atlantic oceans and SH circumpolar low pressure belt. CLDRADI maxima appear over the Indonesian, Atlantic ITCZ, and Indian monsoon regions, though the

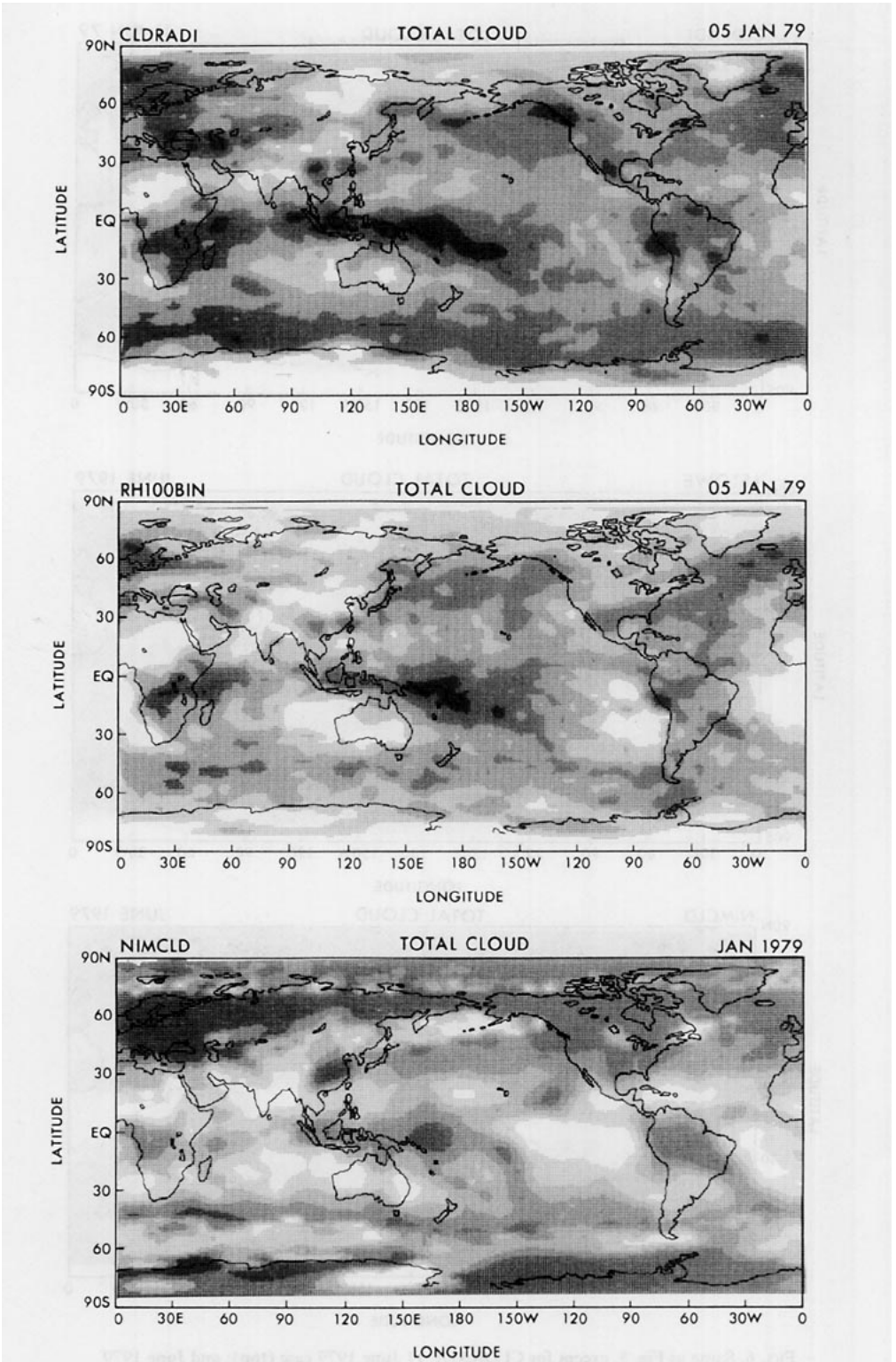

FIG. 5. Thirty-day (days 0–30) mean total cloud amount n_T. CLDRADI, 5 January 1979 case (top); RH100, 5 January 1979 case (middle); NIMCLD, January 1979 monthly mean (bottom). Stippling: none for $0 \leq n_T \leq 0.20$; progressively darker stippling for the (0.20, 0.40), (0.40, 0.60), (0.60, 0.80), and (0.80, 1.00) cloud fraction intervals.

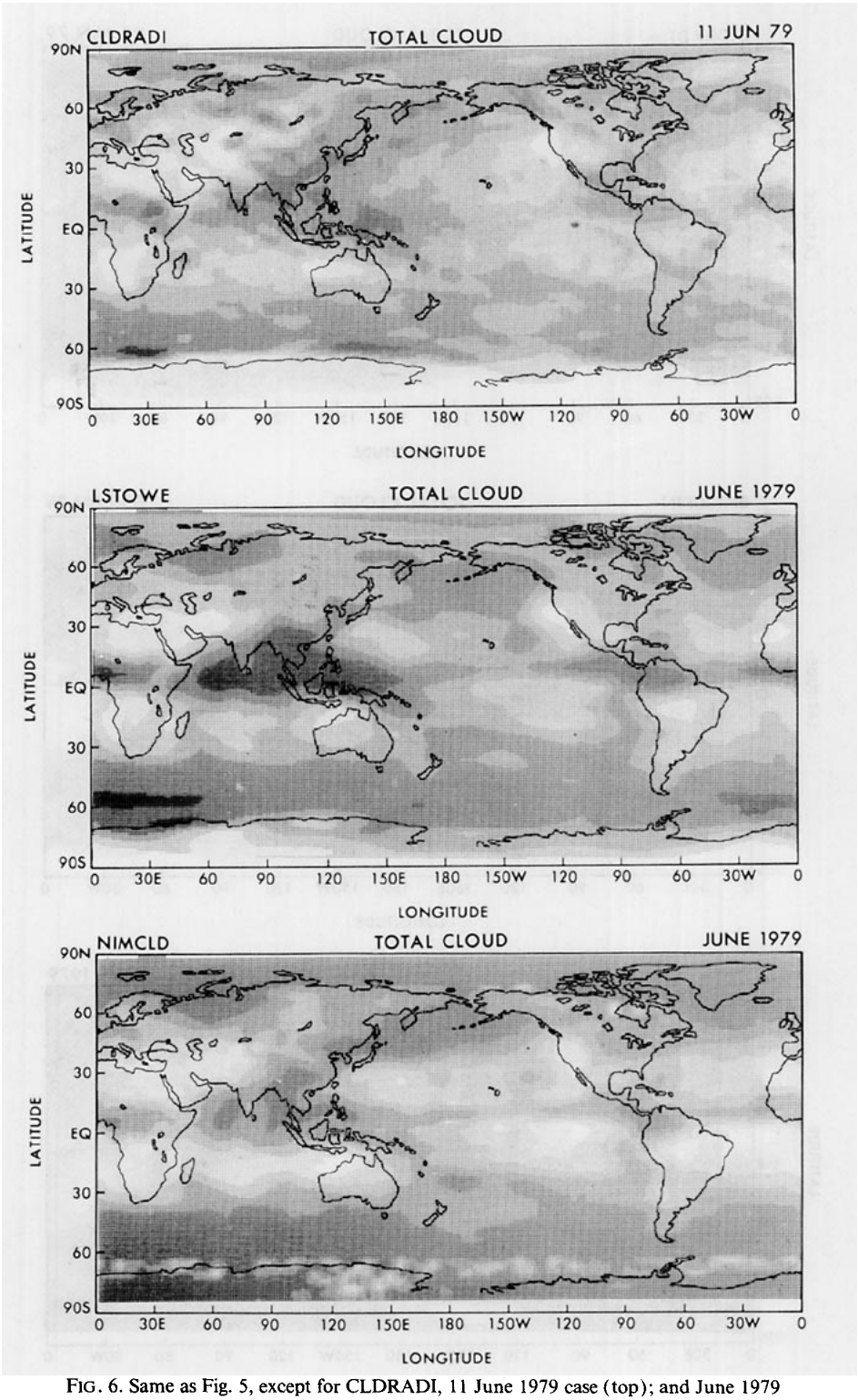

FIG. 6. Same as Fig. 5, except for CLDRADI, 11 June 1979 case (top); and June 1979 monthly means for STOWE (middle) and NIMCLD (bottom).

latter two maxima are weaker than STOWE's. Equatorward of 45°, the STOWE and NIMCLD large-scale features resemble each other, lending some credence to the NIMCLD effective total cloud amount data. (At high latitudes, especially in the polar night region, the algorithm for NIMCLD effective cloud amount is not

meaningful.) All three panels indicate a minimum of total cloudiness off the coast of California during June–July 1979.

The qualitative agreement between predicted versus observed total cloud amount extends to high clouds (not shown), especially at low latitudes. In contrast, there is less correspondence for low and middle clouds (not shown), consistent with Slingo (1987), who cited the use of different definitions of low versus middle clouds as a contributing factor. CLDRADI middle clouds stretch across much of the North Atlantic and Pacific oceans and the 50°–60°S latitude belt; and in the tropics, middle cloud patterns resemble high cloud patterns. Considerably more middle cloud is produced in CLDRADI than in RH100. CLDRADI, NIMCLD, and STOWE all indicate weak stratus activity off the California coast during June–July 1979, though CLDRADI and NIMCLD produce some stratus off the west coast of South America in January 1979. Our model's tendency to generate excessively low relative humidities in the planetary boundary layer near the west coasts could reduce the amount of stratus [see Eq. (9)].

CLDRADI seems to underpredict low and/or middle cloud amount over the subtropical and extratropical oceans, including the North Atlantic and Pacific, and near the SH circumpolar low pressure belt. We speculate that this behavior is due to multiple causes. First, Slingo's scheme is not "perfect," nor have its parameters been explicitly retuned to our model. Second, our model, like other models, exhibits substantial systematic biases, for example, in the planetary boundary layer; and it tends to underestimate the transient eddy energy and intensity of midlatitude synoptic disturbances. As already shown in Fig. 4, predicted cloud amount is quite sensitive to the GCM's spectral resolution at polar latitudes. The cloud prediction could be improved by reducing the model's systematic biases, as well as optimizing the parameters of the cloud formation algorithm for the GCM. Third, the discrepancy between different "observations" is not small compared to that between model and observation (cf. Fig. 3). This could cause a model's cloud-verification results to be misinterpreted in some instances. Also, we suspect that the optical depths of CLDRADI clouds are too thin over the aforementioned extratropical regions, based upon a preliminary comparison with ISCCP C2 data.

6. Radiative response

The TOA ERB response to cloud–radiation interaction is verified against observation. Then, the OLR response to anomalous surface boundary forcing and the in situ atmospheric radiative response to cloud–radiation interaction are described. Moderate OLR and upper-tropospheric cirrus-warming responses occur in the tropics.

a. Top-of-the-atmosphere response to cloud–radiation interaction

Two cases, 5 January 1979 and 11 June 1979, are highlighted, because their forecast periods should be better synchronized in time with monthly mean verification data and/or are centered closer to a solstice, compared to the other cases. Also, the 15 July case is briefly discussed, since ERBE verification data were available. Disregarding some intercase variability associated with the seasonal trend in incoming solar radiation, anomalous surface boundary forcing, etc., the predicted ERB fields for the previously cited cases qualitatively resemble the respective three-case winter and summer case ensemble means.

CLDRADI 30-day mean (days 0–30) OLR fields for the 5 January 1979 and 11 June 1979 cases are verified against *Nimbus-7* monthly mean observations in Figs. 7 and 8, respectively. LONDON is included in Fig. 7 to dramatize that CLDRADI's OLR field is much more zonally asymmetric than LONDON's in the tropics and subtropics. OLR variations are controlled mainly by cloud variations in this region, and the LONDON clouds are zonally symmetric. (LONDON's weak longitudinal variations in OLR are related to those in water vapor and/or temperature.) In the NH winter extratropics, where the longitudinal variation in OLR is controlled more by variations in surface temperature and less by variations in cloud cover, CLDRADI and LONDON are comparably asymmetric. Returning to the tropics, CLDRADI's OLR field bears closer resemblance than LONDON's, overall, to observation, as expected. Low values of CLDRADI OLR (e.g., in Fig. 7) tend to correspond to large values of total and high cloud amount. In January, the observed ITCZ and SPCZ are qualitatively simulated by CLDRADI. But the OLR minimum over the central Pacific is displaced southeast of the observation and CLDRADI fails to capture the intensity of the observed OLR minimum over the Amazon. The CLDRADI minimum along the Peruvian coast is orographically induced. In June, CLDRADI is partially successful at simulating the observed monsoon-related OLR features over the Indian Ocean, Bay of Bengal, and southeast Asian regions. However, the simulation is not very good over the NH subtropical west-central Pacific Ocean. Also, over the equatorial central Atlantic and equatorial eastern Pacific oceans, the ITCZ fizzles out in CLDRADI's OLR field. The fact that CLDRADI's total cloud amount field (Fig. 6) displays a more coherent ITCZ there is not really contradictory. First of all, in the tropics, OLR is much more sensitive to high cloud amount (and emissivity) than to low cloud amount. Second, a fair amount of low cloud but not very much high cloud forms in the latter two regions, and the high cloud emissivity is relatively weak there. One speculation is that the model's penetrative convection is too weak over the equatorial central Atlantic and equatorial

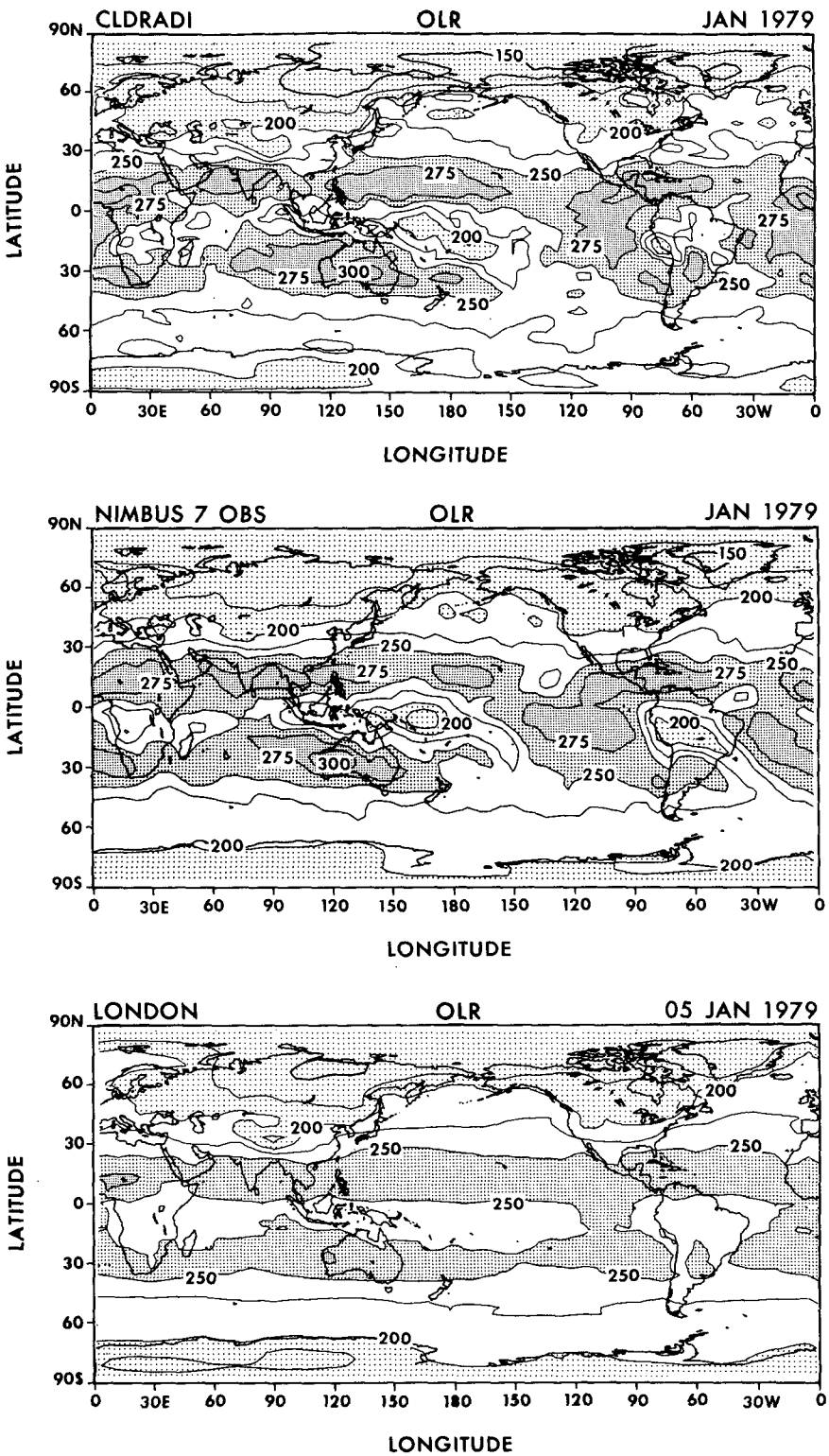

FIG. 7. OLR fluxes. Thirty-day (days 0–30) means, 5 January 1979 case: CLDRADI (top) and LONDON (bottom); and January 1979 monthly mean *Nimbus-7* observations (middle). Contour interval = 25 W m^{-2}. Stippling: <200 W m^{-2}, coarse; 250–275 W m^{-2}, medium; >275 W m^{-2}, fine.

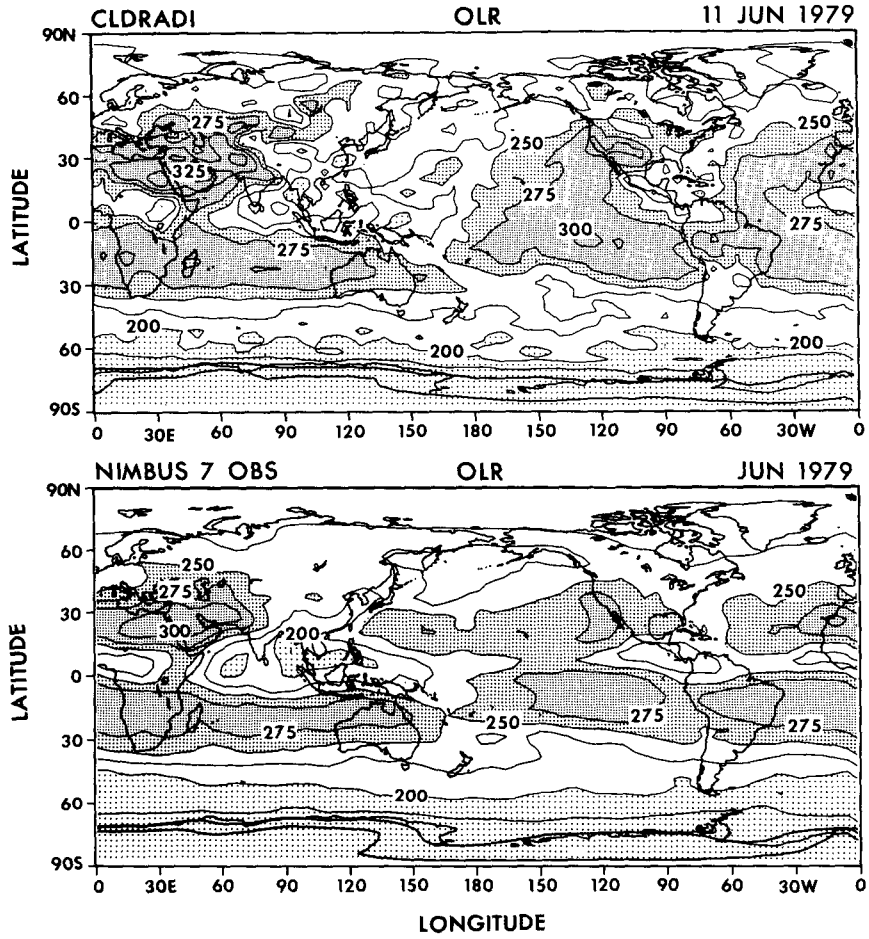

FIG. 8. Same as Fig. 7, except for 11 June 1979 case: CLDRADI (top) and June 1979 monthly mean *Nimbus-7* observation (bottom).

eastern Pacific. When the model's resolution is increased from R21L18 to R42L18, a narrower, more continuous ITCZ is visually detectable in the low and total cloud amount fields, but not in the high cloud amount or OLR fields.

For completeness, the CLDRADI 30-day mean OLR prediction for the 15 July 1985 ERBE case (15 July–13 August) is verified against the July 1985 monthly mean ERBE NFOV OLR in Fig. 9, despite the 15-day lag between model output and observation. The CLDRADI OLR is again quite zonally asymmetric; and as before, it is in gross qualitative agreement with observation, in the tropics, though less so than in the 11 June 1979 case. CLDRADI's OLR minimum over the Indian monsoon region is less intense and less well organized than is observed, while the CLDRADI minima over the western tropical Pacific and Africa are located too far east. Also, the Atlantic branch of the ITCZ is not predicted. CLDRADI's cloud OLR forcing field (not shown) proved to be strongly correlated with the corresponding total OLR field, in regions of significant forcing in the tropics. There, discrepancies between model and observation seemed to be attributable more to cloud effects, rather than to clear-sky effects. Of course, cloud forcing is a very useful concept for explaining the role of clouds in the earth's radiation budget (Ramanathan et al. 1989) and for validating GCMs (Kiehl and Ramanathan 1990).

The CLDRADI absorbed shortwave radiative flux field (not shown), like the OLR, exhibits pronounced zonal asymmetry in the tropics and especially in the NH *summer* extratropics, in the 11 June 1979 case. Cloud effects dominate there, since the incoming solar radiation and surface albedo are rather slowly varying in space; and low clouds tend to have more influence than high clouds by virtue of their greater albedos. This may explain why the ITCZ over the central equatorial Atlantic Ocean is actually somewhat better simulated in this field than in the OLR, particularly at R42L18 resolution. Meanwhile, the steep meridional gradient in incoming solar radiation dominates the *SH winter* extratropics.

The CLDRADI net radiative flux field (not shown) is also noticeably zonally asymmetric in the NH sum-

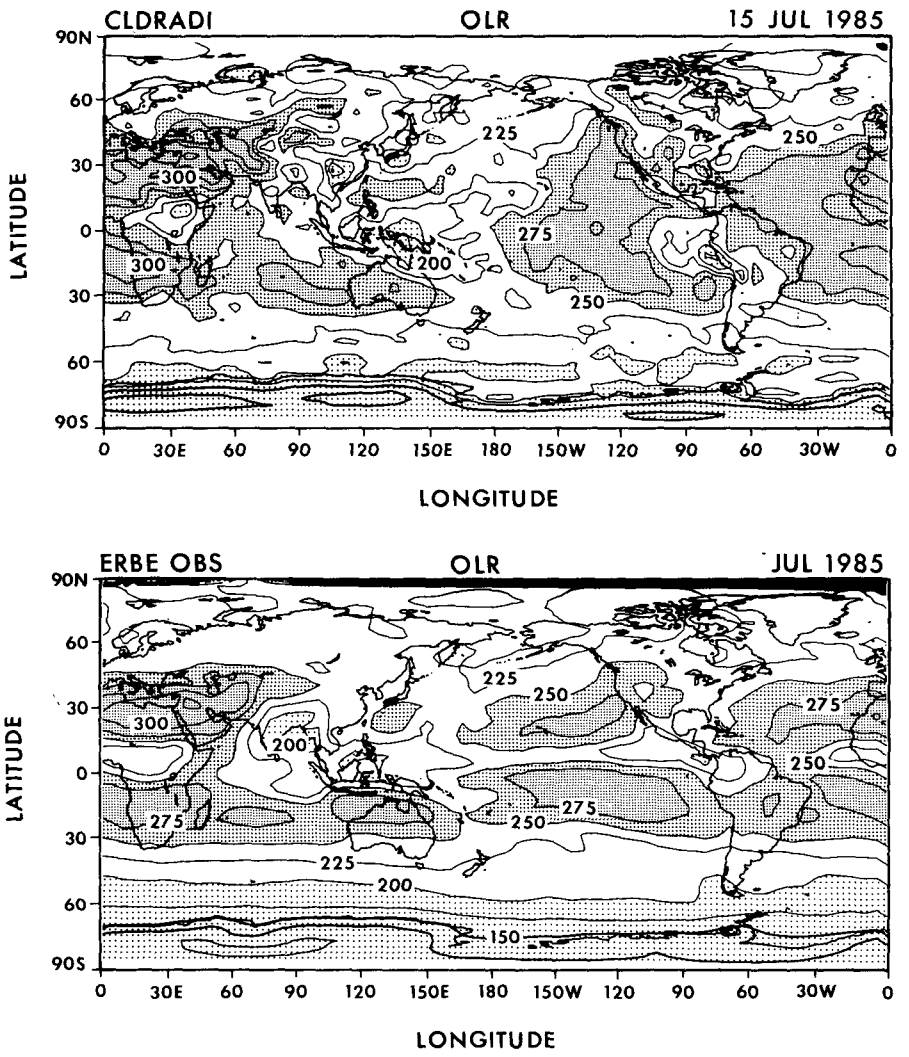

FIG. 9. OLR fluxes. Predicted 30-day (days 0–30) mean, 15 July 1985 case: CLDRADI (top); and July 1985 monthly mean ERBE observations (bottom). Contour interval and stippling as in Fig. 7.

mer extratropics. Conversely, in the ITCZ, asymmetries in absorbed shortwave flux and OLR tend to compensate for each other in both the 11 June 1979 and 15 July 1985 cases, but less so than is observed, and CLDRADI's residual cloud net radiative forcing is larger than ERBE's. The results are qualitatively similar in these latter two respects to those reported by Kiehl and Ramanathan (1990) for the NCAR Community Climate Model.

Zonal-mean biases in predicted OLR, absorbed shortwave radiation, and net radiation fluxes are illustrated in Fig. 10 (5 January 1979 case) and Fig. 11 (11 June 1979 case). There, latitudinal profiles of the 30-day mean, zonal-mean radiative flux differences (forecast minus observation) are plotted for CLDRADI and LONDON. In January, the CLDRADI and LONDON OLR biases are comparable and under 10 W m^{-2}, except at high latitudes. The LONDON bias may be even a few watts per square meter less than CLDRADI's between the equator and 30°N. When the temperature dependence of the cloud optical depth is suppressed (see the CLDRADI-tau curve), the OLR bias flips sign in the tropics and subtropics and its amplitude is reduced within the 0°–10°S latitude belt. In June 1979, the positive CLDRADI and LONDON OLR biases in the ITCZ approach 25 W m^{-2} and are very prominent features of Fig. 11. The CLDRADI bias is smaller than LONDON's, however, in the tropical belt south of the equator.

In January 1979, the LONDON, and even more so, the CLDRADI (or CLDRADI-tau) absorbed shortwave fluxes, seem much too strong in the SH circumpolar low pressure belt and too weak in the tropics. A large high-latitude bias is evident in Harshvardhan et

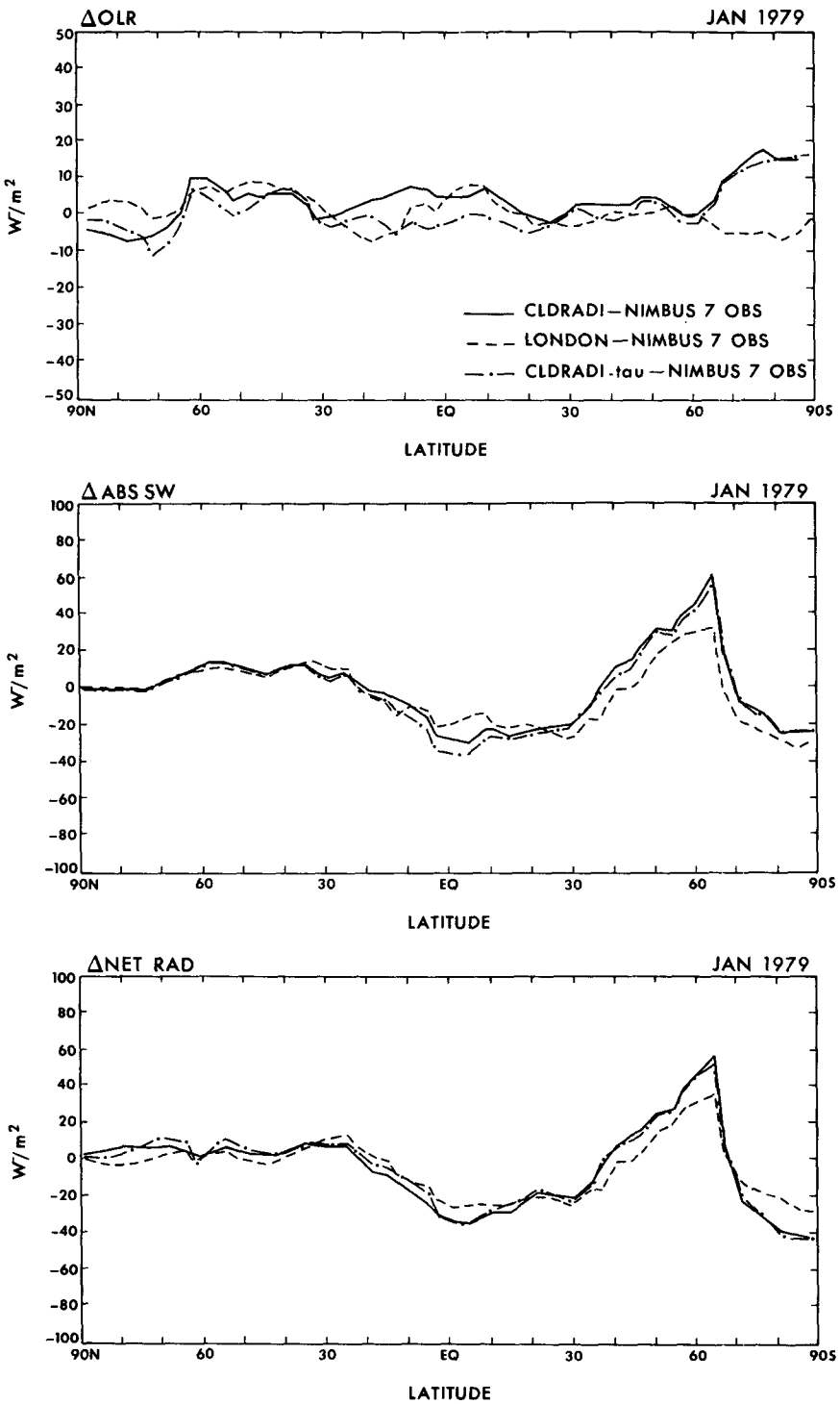

FIG. 10. Time-mean, zonal-mean difference of radiative flux (forecast minus observation) vs latitude. OLR (top), absorbed shortwave (middle), and net radiative flux (bottom). Data based on CLDRADI, LONDON, and CLDRADI-tau 30-day mean forecasts for the 5 January 1979 case and the January 1979 monthly mean *Nimbus-7* observation.

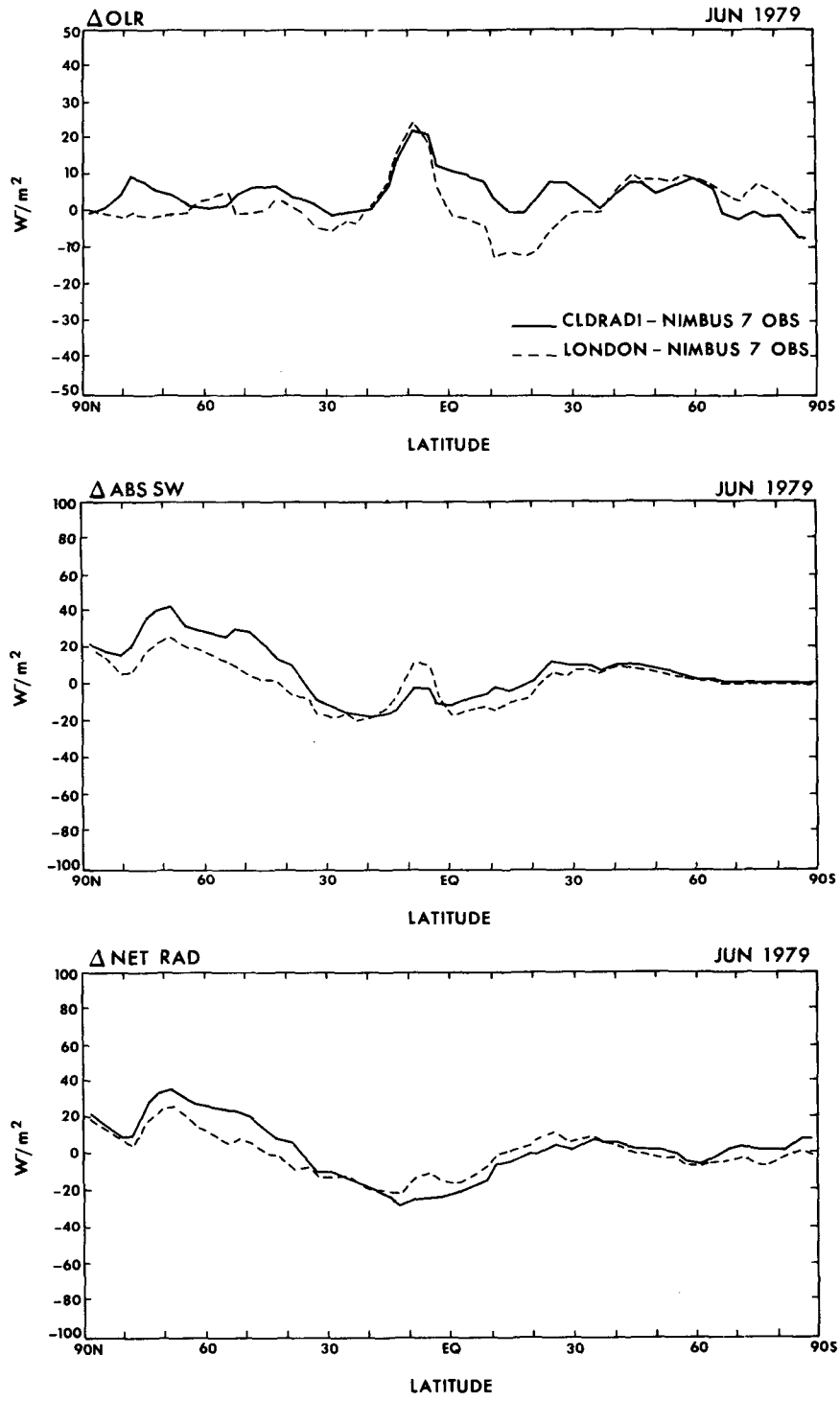

FIG. 11. Same as Fig. 10, except forecasts are for the 11 June 1979 case, observations are June 1979 monthly means, and no curves are plotted for CLDRADI-tau.

al. (1989) as well. CLDRADI-tau has a slightly adverse effect in the tropics, but little effect at high latitudes. A positive bias also occurs in the middle-to-high latitudes during NH summer (Fig. 11), although the peak amplitude for CLDRADI is not so large as in Fig. 10. In January as well as June, the shortwave flux bias is the main contributor to the negative net radiation bias in the tropics and positive net radiation bias in the

high-latitude summer hemisphere. Incidentally, the shortwave radiation biases over the open ocean would have more adverse impact in an ocean–atmosphere coupled GCM than in one such as ours, with specified SSTs.

The causes of the high-latitude radiative-bias problem need to be investigated further. However, in principle, those biases could be reduced by increasing the low and middle cloud amount and the cloud optical depths over the NH and SH extratropical oceans, including the SH circumpolar low pressure belt. Such changes would apparently be justifiable, based upon a preliminary comparison of CLDRADI versus ISCCP C2 zonal mean data.

As for the positive OLR and negative shortwave radiation biases in the tropics, CLDRADI clouds may be too reflective relative to their greenhouse effect. In the 15 July 1985 case, the CLDRADI clear-sky planetary albedo agrees fairly well with the ERBE data, though the clear-sky OLR comparison is less straightforward. In any case, less low and/or more high cloud (amount and/or optical thickness) would probably yield a more realistic tropical radiation budget.

We emphasize that the present cloud–radiation interaction scheme has not reduced our model's *zonal-mean* OLR or absorbed shortwave radiation biases, either in the tropics or at high latitudes. But because the shortwave biases at low and high latitudes are of opposite sign, the predicted planetary albedos are still fairly reasonable. For example, the 30-day means for CLDRADI are 30.8% (5 January 1979 case) and 29.8% (11 June 1979 case), and for LONDON, 31.6% (5 January 1979 case) and 31.2% (11 June 1979 case).

b. *OLR response to anomalous surface boundary forcing during the 1983 El Niño event*

The monthly mean tropical OLR *anomaly* response to globally specified sea surface temperature (SST) forcing is briefly examined in a model with predicted clouds, for a month with highly anomalous forcing. We focus on the month of January 1983, since it coincides with an intense El Niño event. However, the primary objective is to further evaluate the performance of the CLDRADI cloud-formation algorithm.

OLR output was analyzed from a recently completed nine-case ensemble of multiyear climate runs of the CLDRADI-scg T30L18 model, integrated from real initial conditions (for a somewhat different purpose). This model has comparable resolution as the CLDRADI R21L18 model, though two modifications have been made to the parameterized physics (see section 4). However, the *tropical OLR anomaly response* from multiyear runs of either model should be qualitatively similar, and more robust than the OLR response from the shorter CLDRADI 30-day winter case runs. In any event, CLDRADI-scg T30L18 monthly mean *anomaly* fields were computed as departures of the relevant nine-case ensemble mean total field from the model's (1981–1988) 8-yr climatology. The nth member of the nine-case ensemble is identified by the date of its initial conditions, 1 January 1979 + $3n$ months.

The January 1983 monthly mean anomalies of predicted OLR and precipitation, as well as observed SST anomalies, derived from an 8-yr (1981–1988) climatology, are plotted in the lower three panels of Fig. 12. The OLR anomalies over the tropical Pacific tend to be negatively correlated with precipitation anomalies and SST anomalies. The correlations are strongest over the eastern equatorial Pacific and over the central Pacific north of the equator. The relationships between tropical OLR, precipitation, and SST are what one might expect. Warm SST anomalies favor enhanced penetrative convection, and hence enhanced precipitation and total (or high) cloud cover. In turn, the enhanced cloud cover is consistent with the reduced OLR.

The predicted OLR anomaly field for January 1983 may be compared to "observation" (top panel of Fig. 12), as plotted on a Mercator map projection, after Ardanuy and Kyle (1986). The general qualitative correspondence between prediction and observation over the tropical Pacific (except over and northwest of Australia) and Atlantic oceans, Africa, and Brazil is encouraging. However, the maximum amplitude of the predicted OLR anomalies is $\sim$30 W m^{-2} (at least at T30L18 resolution), as compared to $\sim$70 W m^{-2} for the observed. Perhaps 15–20 W m^{-2} of the apparent discrepancy can be attributed to differences between the "observed" climatology (which is based on the three pre–El Niño Januarys, 1980, 1981, and 1982), and the predicted 8-yr climatology (which spans two major El Niño events).

The predicted OLR anomaly pattern during the January 1987 El Niño (not shown) resembles that of January 1983, though the amplitude over the eastern equatorial Pacific is not as intense. Conversely, the anomaly pattern during the La Niña month of January 1984 (not shown) resembles the mirror image of the January 1983 pattern.

c. *Tropospheric response to cloud–radiation interaction*

The GCM's in situ atmospheric radiative response is interesting, though we lack verification data. We focus on the tropical upper troposphere, and on low cloud-top levels in the middle to lower troposphere.

CLDRADI and LONDON winter ensemble 20-day mean (days 10–30), zonal-mean longwave radiative heating rates are plotted in the latitude–σ plane in Fig. 13. A blob of CLDRADI longwave heating in the tropical stratosphere penetrates downward into the upper troposphere. A modestly greater amount of high cloud amount (compared to LONDON) and the tendency

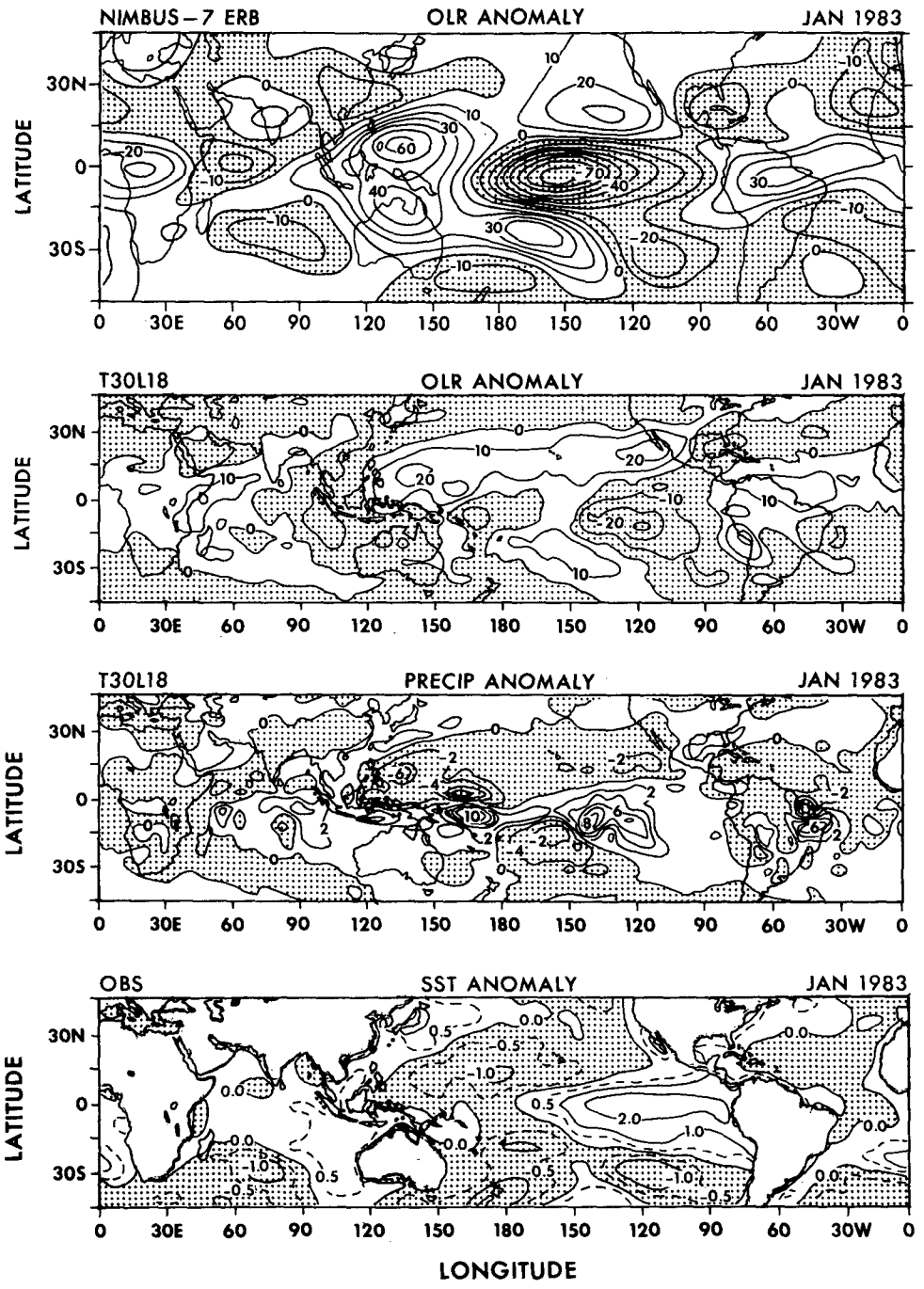

FIG. 12. January 1983 monthly mean anomalies. "Observed" OLR, after Ardanuy and Kyle (1986) (top panel); CLDRADI-scg T30L18 predicted OLR (second panel), and precipitation (third panel); observed SST (bottom panel). Contour intervals: OLR = 10 W m^{-2}; precip = 2 mm day^{-1}; SST = 1 K day^{-1}. Negative anomalies are stippled.

of CLDRADI high clouds to form over a range of σ levels are controlling factors. In LONDON, the positive heating is confined to the lower stratosphere, two sigma levels above the high cloud layer at $\sigma = 0.223$, and is thus not cloud related. A maximum (CLDRADI − LONDON) differential zonal-mean *response* of ~0.5 K day^{-1} occurs in the tropics near $\sigma = 0.156$.

The longitudinal response (not shown) is somewhat more dramatic. CLDRADI "hot spots" are negatively correlated with longitudinal variations in OLR and

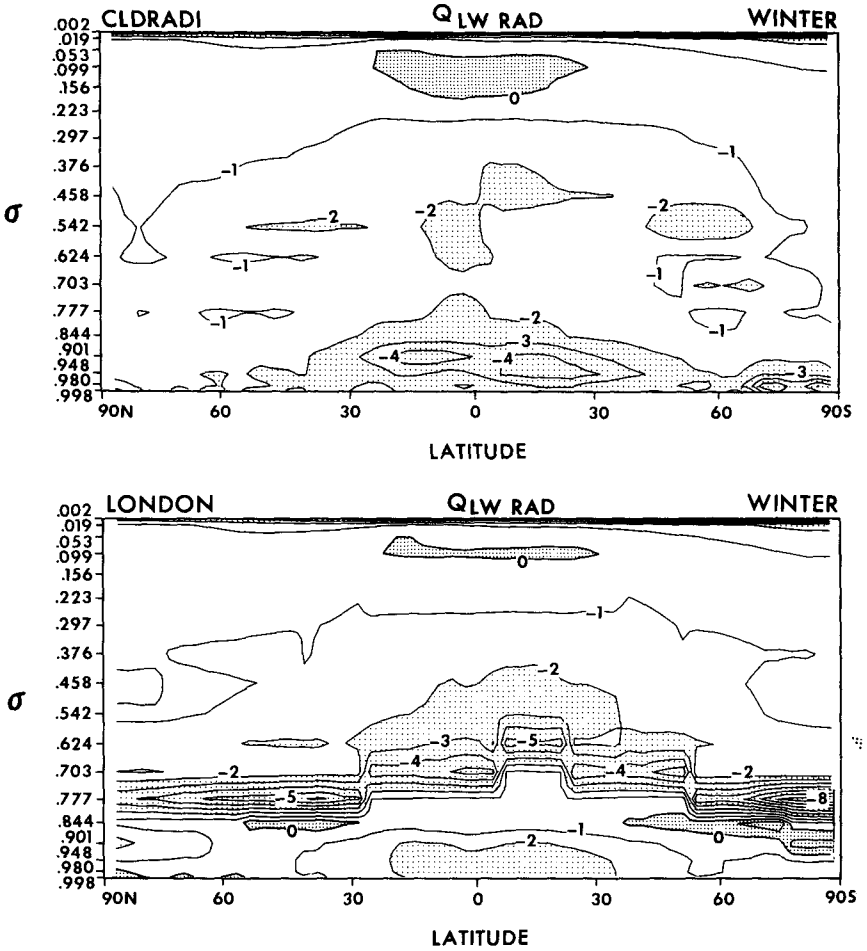

FIG. 13. Twenty-day (days 10–30) ensemble-mean, zonal-mean longwave radiative heating rates for winter. (a) CLDRADI and (b) LONDON. Contour interval = 1 K day^{-1}. Stippling: coarse, < −2 K day^{-1}; fine, >0 K day^{-1}.

span a few sigma levels. Over the western and central Pacific, its longwave heating-rate maxima approach 2.5 K day^{-1} at $\sigma = 0.156$; and CLDRADI-tau exhibits even stronger longwave heating. LONDON's heating of ~1.5 K day^{-1} at $\sigma = 0.223$, near the Andes, is due to locally colder (cloud-top) temperatures on this sigma surface. Meanwhile, CLDRADI's shortwave heating rates are only O(20%–25%) of the longwave values, and longwave heating is the dominant contributor to the net radiative heating.

In the middle-to-lower troposphere, LONDON exhibits more intense longwave cooling than CLDRADI, and its sharp meridional gradient coincides with the gradient in the vertical placement of LONDON's fixed cloud tops. LONDON's zonal-mean OLR bias may be reduced slightly by this cooling. In the extratropics, longwave cooling rates of ≥4–5 K day^{-1} occur at LONDON low cloud tops versus 1–2 K day^{-1} at CLDRADI's. Also, at higher latitudes, the respective vertical profiles are quite different. Meanwhile, in the tropics, LONDON exhibits ~5 K day^{-1} cooling at ~600–700 hPa versus ~4 K day^{-1} for CLDRADI near 900 hPa. But the CLDRADI low cloud-top longwave cooling overlaps with the water vapor longwave cooling. The latter is of O(2 K day^{-1}) below 900 hPa, as one may infer from the bottom panel of Fig. 13. Thus, even in the tropics, the contribution of the CLDRADI low clouds to longwave cooling is only ~2 K day^{-1}. With parameterized shallow convection, the predicted low cloud tops and their associated longwave cooling shift upwards to ~750 hPa in the tropics, and the water vapor longwave cooling is weaker at this level.

The CLDRADI–LONDON lower-tropospheric longwave radiative response is quite large. Yet only ~25% of it is directly related to differences in low cloud amount and properties. The rest is an artifact of a previous code revision, whereby explicit vertical smoothing of the in-cloud longwave cooling profiles was eliminated from the radiation code for being ad hoc. Such smoothing reduces the longwave cooling at the tops of

thick low clouds, that is, clouds straddling two or more layers. LONDON's low clouds are more sensitive than CLDRADI's to the explicit vertical smoothing. First, LONDON's are *always* two layers thick, whereas CLDRADI's are frequently only one layer thick. Moreover, CLDRADI time–zonal-mean longwave cooling profiles are implicitly smoothed in the vertical anyway (cf. Fig. 2), since the vertical placement of its clouds is time and longitude dependent.

When the in-cloud vertical smoothing was restored in LONDON-adj (not shown), the maximum cooling decreased from $\sim$5.5 K day^{-1} (in LONDON) to $\sim$2.5 K day^{-1} equatorward of latitude 60°. Actually, the LONDON longwave cooling at low cloud-top level is unrealistically intense, given the GCM's vertical resolution. Longwave cooling of $\sim$20 K day^{-1} may be quite reasonable, if confined to the top 30 m of a cloud. Extrapolating to coarser resolution, one might expect $\sim$5 K day^{-1} cooling for a σ layer $\sim$120 m thick, but only $\sim$1 K day^{-1} for a σ layer $\sim$600 m thick, that is, the resolution of our 18-level GCM near 700 hPa. Explicit vertical smoothing will be restored as the default in future 18-level versions of the model.

Despite the rather large nir absorptivity of CLDRADI low clouds (Fig. 1 and Table 2), the CLDRADI–LONDON differential zonal-mean shortwave radiative heating response was quite weak in the lower troposphere, attaining a maximum of $\sim$0.25 K day^{-1} in the tropics near 950 hPa.

7. Thermal response

The CLDRADI–LONDON day 10–30 ensemble-mean, zonal-mean temperature differences are examined first. Encouragingly, their extremes tend to be statistically significant, despite the small number of cases. Cloud–radiation interaction appears to have favorable impact on the zonal-mean systematic temperature error in the tropics and over Antarctica.

a. Zonal-mean differences

As mentioned in section 4, 20-day means for days 10–30 are taken for zonal mean differences as well as errors, to minimize spinup effects. Three sets of 20-day ensemble-mean zonal-mean temperature differences $\Delta\langle T\rangle$ for NH winter are plotted in the latitude–σ plane in Fig. 14: CLDRADI − LONDON (top panel), and to help interpret the results, LONDON-adj − LONDON (middle panel) and CLDRADI-tau − LONDON (bottom panel). Recall that CLDRADI-tau is the same as CLDRADI, except that the Harshvardhan et al. (1989) temperature-dependent formula for the optical depth of cold clouds is suppressed; fixed values for warm high, middle, or low clouds are used instead. The effect is to increase the optical depth of high clouds. Zonal means are denoted by angle brackets. The 95% confidence level for nonzero mean differences, as estimated from Student's t-test, for $N = 3$ cases, is exceeded in finely stippled regions of positive differences and in crosshatched regions of negative differences. Coarse stippling delineates negative $\Delta\langle T\rangle$ values that fail the above significance test.

Two prominent features of the CLDRADI–LONDON differential response are the upper-tropospheric (anvil) cirrus warming in the tropics, which extends into the lower middle latitudes, and a lower tropospheric warming. It is instructive to compare the NH winter temperature differences to the atmospheric zonal-mean radiative heating and cooling rates, shown in Fig. 13. The regions of warming in Fig. 14 correspond closely to the regions of positive longwave radiative heating differences implied by Fig. 13. In the tropical upper troposphere, the maximum warming is centered near $\sigma = 0.156$ and is statistically significant at the 95% confidence level. The warming exceeds 2 K over quite a wide latitude belt, and values greater than 3 K are found between 15° and 30°S. The $\Delta\langle T\rangle$ response is consistent with a modestly positive CLDRADI–LONDON difference in zonal-mean high cloud amount as well as higher penetration by some of CLDRADI's high cloud tops to $\sigma = 0.156$ (vs $\sigma = 0.223$ for LONDON). The warming response near the tropical tropopause increases by $\sim$2 K, attaining a maximum of $\sim$5 K, when the Platt–Harshvardhan temperature-dependent parameterization of cloud optical thickness is switched off. The CLDRADI and CLDRADI-tau responses are reminiscent of those reported by Ramanathan et al. (1983) for variable nonblack cirrus and for variable black cirrus, respectively. The CLDRADI–LONDON response is qualitatively similar in NH summer (not shown), with the following caveats. The response is somewhat weaker, the statistically significant regions are somewhat smaller, and the latitude belt of maximum warming shifts northward.

Lower in the troposphere, Fig. 14 (top panel) reveals a rather intense CLDRADI–LONDON warm band response centered at the σ level of the LONDON low cloud tops, and extending from pole to pole. Local maxima exceed 4 K in the tropics and midlatitudes and 8 K near the North Pole. The response seems to be statistically significant at most latitudes in NH winter, and at tropical and NH latitudes in NH summer. However, *equatorward of latitude 60°*, it is mainly an artifact of the vertical smoothing of the in-cloud longwave cooling profile (discussed in section 6), as can be inferred from a comparison of the top and middle panels of Fig. 14.

Focusing next on Antarctica, we see that a statistically significant CLDRADI–LONDON cooling response in $\Delta\langle T\rangle$ occurs in the lower troposphere during SH summer. Comparison with the CLDRADI versus LONDON longwave-cooling rates over Antarctica (in

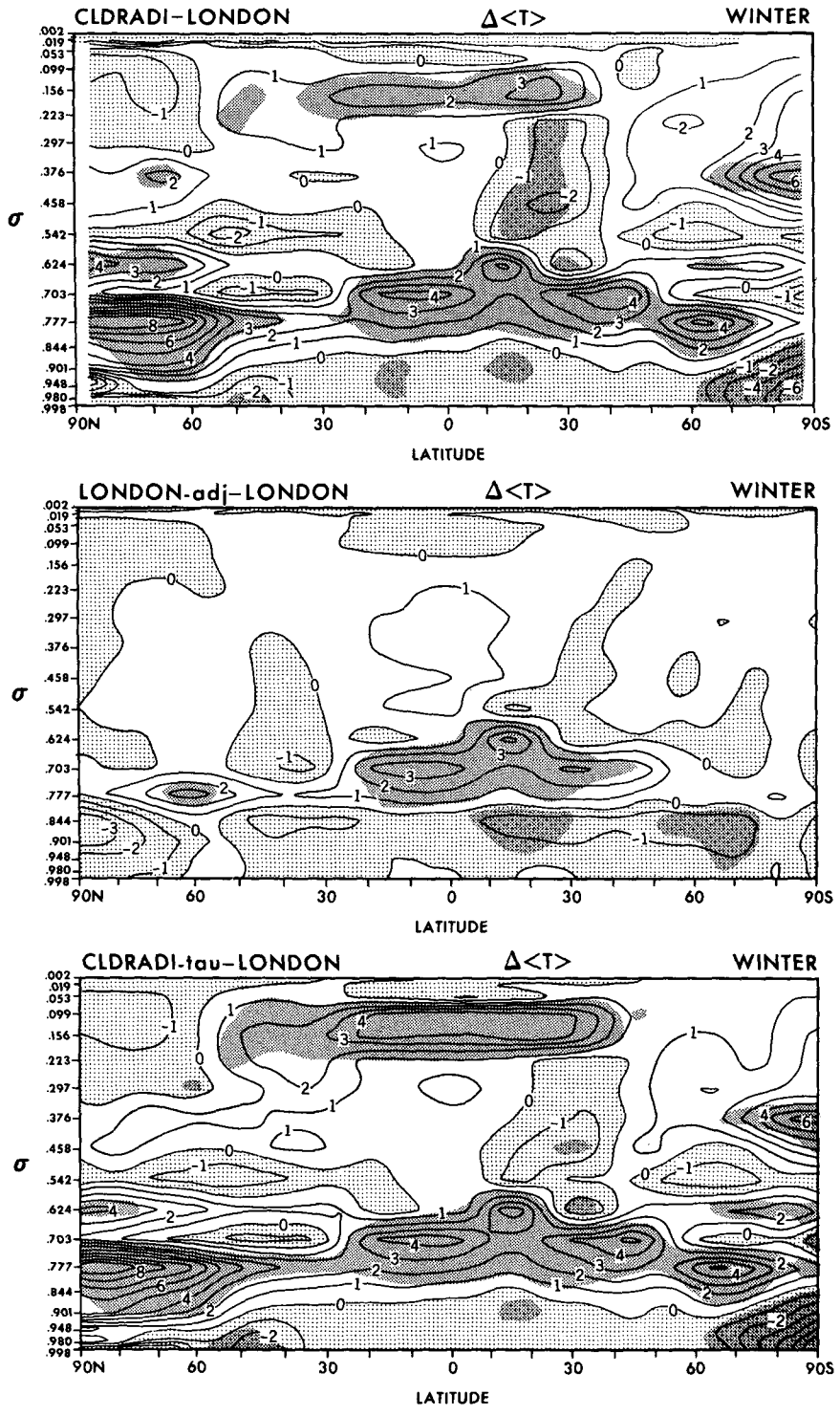

FIG. 14. Twenty-day (days 10–30) ensemble-mean, zonal-mean temperature differences for NH winter. CLDRADI − LONDON (top); LONDON-adj − LONDON (middle); CLDRADI-tau − LONDON (bottom). Contour interval = 1 K. Stippling: $\Delta < T >$ negative, coarse; $\Delta < T >$ negative and statistically significant, crosshatched; $\Delta < T >$ positive and statistically significant, fine.

Fig. 13) confirms that this response is radiatively driven. Three cloud-related factors play a role here: (i) CLDRADI features less low cloud amount than LONDON over Antarctica; (ii) its low clouds are located in the warmer near-surface layer (cf. Fig. 2), more than 100 hPa beneath LONDON's; (iii) they are optically thinner. Both CLDRADI and LONDON generate positive lapse rates (not shown) in the Antarctic lower troposphere, though CLDRADI's is closer to isothermal. Curiously, CLDRADI and LONDON low clouds radiate at nearly the same temperature, despite the aforementioned differences in their low clouds and vertical temperature profiles. Relatively weaker cooling responses are centered at CLDRADI middle ($\sigma = 0.703$) and high ($\sigma = 0.542$) cloud levels, whereas a strong warming response is centered at the LONDON high cloud level ($\sigma = 0.376$).

The zonal-mean temperature difference $\Delta\langle T\rangle$ reverses sign in the Antarctic lower troposphere in SH winter (not shown), now being strongly positive (with $\Delta\langle T\rangle$ as large as 8 K), and CLDRADI's near-surface inversion is more intense than LONDON's. The $\Delta\langle T\rangle$ maxima are centered at the levels of the LONDON low, middle, and high cloud tops. Little if any CLDRADI cloudiness is found at these levels or any others (cf. Fig. 3) over Antarctica during austral winter. Thus, to a first approximation, CLDRADI may correspond to the clear-sky solution there and the CLDRADI–LONDON temperature difference to the LONDON longwave cloud forcing response (with sign reversed).

The Antarctic SH winter response may occur partially for the wrong reason, since CLDRADI predicts much less total cloud cover over Antarctica than ISCCP does (cf. Fig. 3). There, spectral truncation errors in the water vapor field may cause cloud amount to be underpredicted. The situation could be exacerbated by the colder conditions of SH winter and by coarser model resolution (cf. Fig. 4). But even if there were more cloud cover, the vertical placement of the CLDRADI clouds and their optical thickness might significantly affect the temperature response in the Antarctic lower troposphere. The CLDRADI low clouds form very close to the surface, and optically thin "clouds" have been detected with lidar by Smiley et al. (1980) near the Antarctic surface on frequent occasions between March and November.

b. *Zonal-mean systematic error*

Systematic temperature errors of GCMs become quite well established over the 10–30-day forecast range, as has been well documented in CAS/JSC (1988) and elsewhere. The CLDRADI and LONDON integrations are no exception. We have plotted the CLDRADI and LONDON 20-day (days 10–30) winter ensemble-mean, zonal-mean temperature errors versus latitude and pressure in Fig. 15. Regions of negative temperature error are stippled. In the upper tropical troposphere, especially near the tropopause, the zonal-mean temperature error is typically only -1 to -2 K with cloud–radiation interaction as compared to -3 to -4 K without it, in winter (Fig. 15) as well as summer (not shown). Descending beneath 200 hPa into the middle troposphere, CLDRADI's systematic error still tends to be slightly less than LONDON's in the tropics (north of latitude 20°S), during NH winter. But the reduction in systematic temperature error in CLDRADI's tropical troposphere near 700 hPa, in both seasons, is more striking. As noted earlier, the in-cloud vertical profiles of longwave cooling were not vertically smoothed; and LONDON clouds are more sensitive than CLDRADI clouds to this feature of the radiation code. This explains ~75% of the error reduction. Beneath 850 hPa, where CLDRADI low clouds prefer to form, the cold bias increases from ~1 K in LONDON to 2 K in CLDRADI. But overall, with cloud–radiation interaction, the cold bias is reduced over most of the tropical troposphere.

Although the reduction in the tropical cold bias is encouraging, the results need to be interpreted with caution. Schemes similar to Slingo (1987), such as ours, produce one-layer-thick cirrus and hence longwave radiative warming near 200 hPa, whereas parameterizations of thick anvil cirrus (e.g., Randall et al. 1989) are associated with longwave radiative cooling near this level. On the other hand, with LONDON clouds, Sirutis and Miyakoda (1990) obtained a 2 K monthly mean warm bias at 200 hPa with the Arakawa–Schubert cumulus parameterization, versus a 5-K cold bias with moist convective adjustment. Thus, a warm, radiative bias could compensate for a cold, convective bias or reinforce it, or vice versa, depending how cloud–radiation and cumulus convection parameterizations were paired. Clearly, more validation of tropical cirrus and cumulus convection parameterizations is needed. Observed vertical profiles of radiation fluxes and/or cloud amount and cloud optical depth would be useful for verifying cloud-prediction schemes in the tropics, as well as over Antarctica and elsewhere.

Speaking of Antarctica, beneath ~500 hPa, the model's long-standing *SH summer warm bias* (Fig. 15) is reduced from ~4–6 to ~2–4 K, that is, by ~2 K by cloud–radiation interaction; and the *SH winter cold bias* (not shown) is reduced even more drastically, from ~9 to 2 K poleward of 75°S. Differences in cloud amount (CLDRADI has very little during SH winter), its vertical placement, and cloud optical depth are the controlling factors through their effects on the IR emission.

8. Zonal-wind response

CLDRADI and LONDON ensemble mean latitude–height cross sections of zonal wind (for NH winter) are compared against NMC observations in Fig. 16.

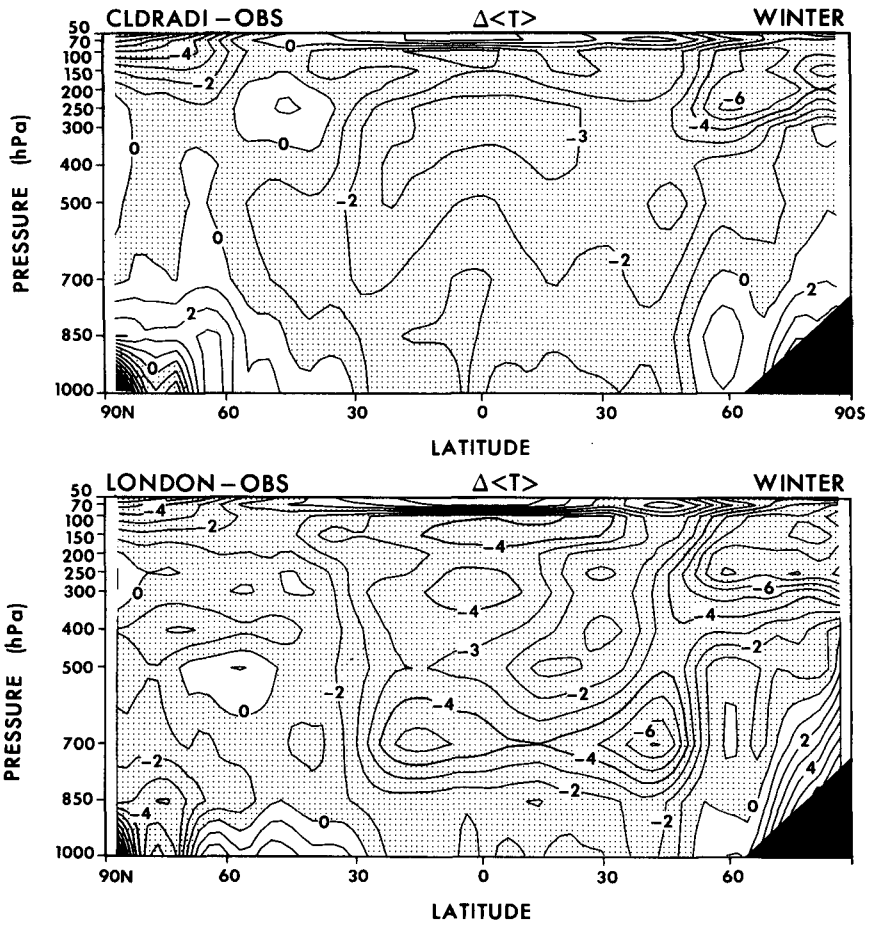

FIG. 15. Twenty-day (days 10–30) ensemble-mean, zonal-mean temperature error for NH winter. CLDRADI (top); LONDON (bottom). Contour interval = 1 K. Negative errors are stippled.

Like observation, CLDRADI exhibits zonal-mean westerlies in the upper tropical troposphere, which are stronger than observed, whereas LONDON exhibits easterlies. This contrasting feature may have some significance for the SH summer midlatitude geopotential height response, discussed in section 10. Second, the latitudinal position and especially the amplitude of the CLDRADI SH summer westerly jet verifies better than LONDON against observation. On the other hand, CLDRADI's NH midlatitude westerlies extend too far equatorward.

CLDRADI–LONDON zonal-wind differences $\Delta\langle u\rangle$ are shown in Fig. 17 for NH winter. A statistically significant westerly acceleration occurs in the tropical upper troposphere, where the maximum $\Delta\langle u\rangle$ exceeds 10 m s^{-1}. But CLDRADI's systematic zonal-wind error (not shown) is comparable to LONDON's in magnitude, though of opposite sign. Some statistically significant decelerations are found in the SH summer midlatitude mid-to-upper troposphere and in the NH winter 50°–60°N belt. The meridional structure of the tropical–SH extratropical responses resembles that obtained in the anomaly forcing experiments of Ting and Held (1990) and may represent some kind of normal mode. The tropical and SH extratropical wind responses are in approximate geostrophic balance with the meridional temperature gradients, induced by cloud–radiation interaction, which flank the negative temperature differences in the SH tropical middle troposphere (cf. top panel of Fig. 14). In NH summer (not shown), the tropical acceleration is weaker, consistent with its northward displacement and the geostrophic thermal wind relation. The amplitude of the LONDON-adj–LONDON differential equatorial acceleration (not shown) is only half as large as CLDRADI–LONDON's and there is virtually no SH summer midlatitude deceleration. Thus, half of the CLDRADI–LONDON differential equatorial westerly acceleration and nearly all of the SH midlatitude deceleration responses seem to be radiatively driven by cirrus heating in the tropical upper troposphere. The remainder may be linked to the weaker radiative cool-

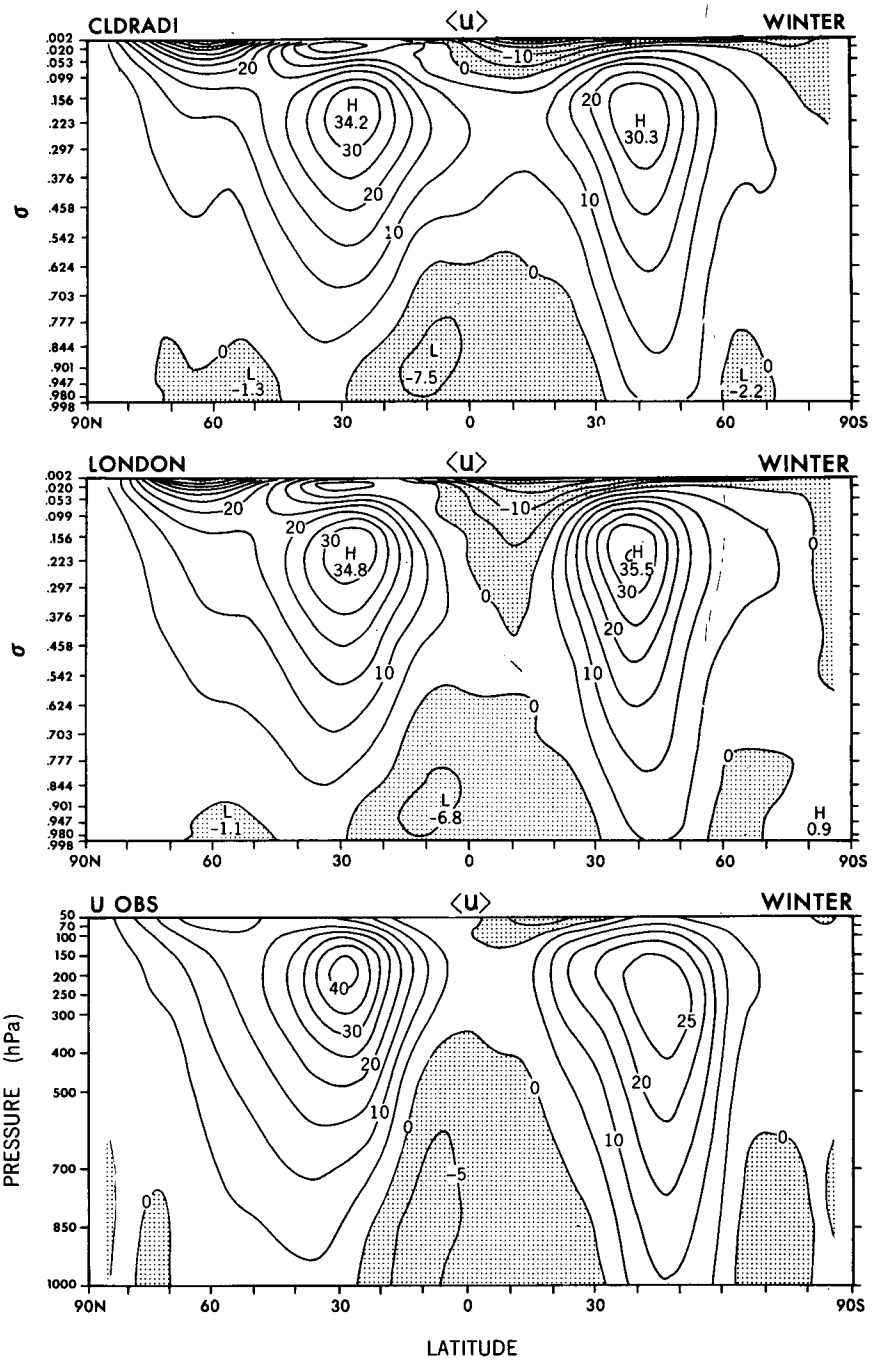

FIG. 16. Twenty-day (days 10–30) NH winter ensemble-mean, zonal-mean zonal wind. CLDRADI (top), LONDON (middle), NMC observations (bottom). Contour interval = 5 m s^{-1}. Easterlies are stippled.

ing at LONDON low cloud-top level in the LONDON-adj and CLDRADI integrations.

9. Geopotential height response

Twenty-day ensemble-mean CLDRADI and LONDON forecasts of geopotential height at 500 and 1000 hPa, z_{500} and z_{1000}, were compared with NMC observation for winter and summer. In the NH (not shown), the CLDRADI and LONDON forecasts are both dominated by large-amplitude, mainly positive errors at high latitudes; at 1000 hPa, these errors are associated with excessive damping of the surface westerlies by the *linear* gravity-wave-drag scheme.

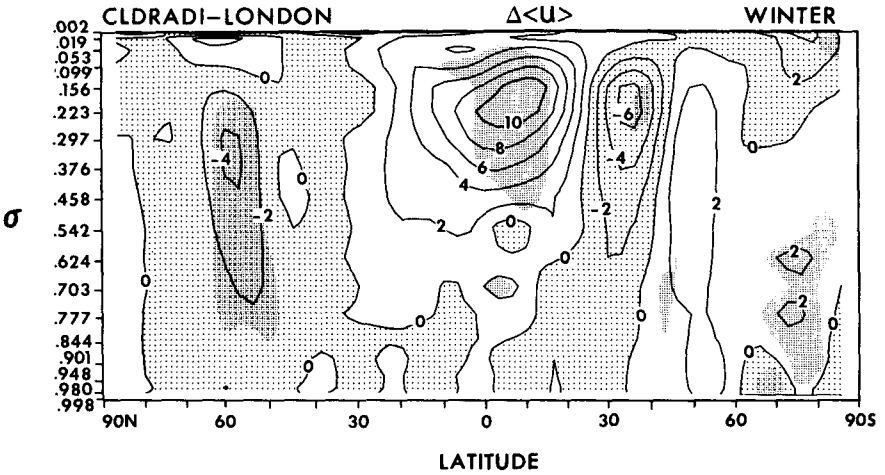

FIG. 17. Same as top panel of Fig. 14, except for zonal-mean zonal-wind differences. Contour interval = 2 m s^{-1}.

Perhaps the most interesting result is that the amplitude of the predicted SH quasi-stationary planetary waves is visibly enhanced in CLDRADI during austral summer, especially for zonal wavenumbers 1 and 3. This may be seen by comparing the CLDRADI, LONDON, and observed 10–30-day ensemble mean z_{500} maps in Fig. 18; a similar response was detected at 1000 hPa. Also, the minimum in zonal-mean sea level pressure associated with the circumpolar low near 60°S intensified by 5 hPa, from 998 hPa in LONDON to 993 hPa in CLDRADI. The strengthening of the zonal circulation is somewhat reminiscent of the SH summer extratropical response obtained by Meehl and Albrecht (1988), when the tropical diabatic heating in their GCM was enhanced by a new parameterization of tropical convection. Nonetheless, the CLDRADI forecast, like LONDON, still suffers from large, positive height errors poleward of 60°S, which are flanked on the north by negative errors, especially near 40°–45°S.

Meanwhile, during austral winter, LONDON's SH quasi-stationary planetary wave activity at 500 hPa (not shown) is considerably more intense than during SH summer, especially at wavenumbers 1 and 4. Although CLDRADI's wave activity is now somewhat less intense than LONDON's and projects more onto wavenumber 3 than 4, these characteristics are actually more consistent with observation according to Karoly (personal communication, 1990).

Ensemble-mean correlation coefficients between the 10-, 20-, and 30-day mean predicted versus observed z_{500} and z_{1000} anomalies have been computed for the 25°–90°N and 25°–90°S extratropical belts. Cloud–radiation interaction had a marginally favorable impact on the first 10-day mean (days 0–10), as well as on the 20- and 30-day means in NH winter and SH summer. While its statistical significance is not assured, the 10-day mean anomaly correlation response is at least consistent with the ECMWF model's medium-range forecast response obtained by Slingo (1987). Perhaps the impact of cloud–radiation interaction is masked by stronger longitudinally asymmetric forcings, especially in the NH and/or by other sources of forecast error. Eventually the latter would cause even a good cloud-prediction scheme to generate clouds at the wrong location and/or time, with further adverse consequences. Moreover, deficiencies in the cloud-prediction scheme itself could interact by amplifying biases in the GCM's radiative budget.

a. Further analysis of the SH summer extratropical quasi-stationary eddy response

CLDRADI, LONDON, and observed Fourier spectra of the eddy geopotential height at 200 hPa, z'_{200}, are plotted in Fig. 19, for the 41°–68°S extratropical latitude belt and austral summer. As usual, *eddy* refers here to the departure from the zonal mean. The results confirm the amplification of the quasi-stationary waves in the SH summer extratropical upper troposphere of CLDRADI. Indeed, CLDRADI nicely reproduces the observed spectrum of z'_{200}, including the peaks at zonal wavenumbers $m = 1$ and $m = 3$. In contrast, LONDON's peaks at $m = 1$ and $m = 3$ are much weaker, and the spectrum is flatter. Descending lower into the atmosphere (not shown), CLDRADI continues to exhibit a more distinct peak at $m = 3$ than LONDON, though below 400 hPa, the LONDON spectrum contains slightly more variance at $m = 3$ than CLDRADI.

Spectra of predicted tropical eddy diabatic heating Q' for austral summer and two latitude domains, 2°N–9°S and 12°–28°S, are displayed in Fig. 20. At levels $\sigma_5 = 0.156$ and $\sigma_6 = 0.223$, where the CLDRADI and LONDON longwave radiative heating each attain their

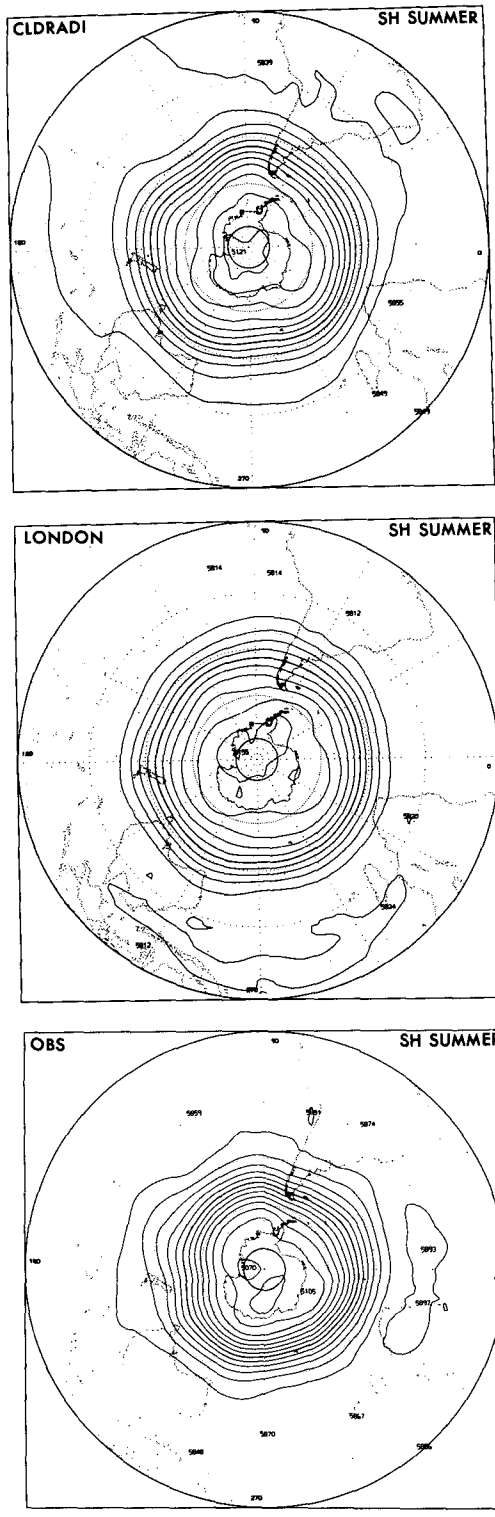

FIG. 18. Twenty-day (days 10–30) SH summer ensemble-mean geopotential height at 500 hPa. CLDRADI (top) and LONDON (middle); NMC observations (bottom). Contour interval = 6 dam. Reference contour = 0 dam.

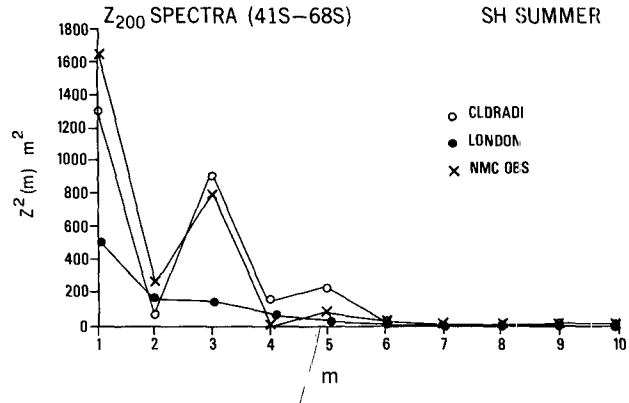

FIG. 19. Twenty-day (days 10–30) ensemble-mean z'_{200} eddy geopotential height spectra vs zonal wavenumber for the 41°S–68°S SH summer extratropical latitude belt. CLDRADI, LONDON, and NMC observed spectra.

relative maximum, the eddy diabatic heating rates are quite modest, though CLDRADI's is somewhat stronger of the two. Its most prominent Q'_5 peaks in the 2°N–9°S and 12°–28°S domains occur at wavenumbers 1 and 3, respectively, with amplitudes of ~0.45 and ~0.30 K day^{-1} compared with ~0.28 and ~0.18 K day^{-1} for LONDON's Q'_6 peak. Thus, eddy diabatic heating may be capable of forcing weak wavenumber 1 and 3 disturbances in either model. If so, another factor is still needed to explain the amplitude of the z' spectral response in Fig. 19.

The zonal-mean wind conditions in the SH summer tropics and subtropics are a plausible candidate. Referring again to Fig. 16, in the tropical upper troposphere, CLDRADI exhibits rather strong zonal-mean westerlies whereas LONDON exhibits zonal mean easterlies. CLDRADI's westerlies there should tend to favor the meridional propagation of quasi-stationary wave activity to the SH extratropics, whereas the LONDON easterlies should tend to inhibit it. Eddy diabatic heating is more intense in the tropical middle troposphere, where latent heating (not shown) dominates, than in the upper troposphere, and LONDON's is somewhat stronger than CLDRADI's. But the zonal-mean westerlies are weaker, and LONDON's are weaker than CLDRADI's. Zonal-mean tropical easterlies are found below 600 hPa in both predictions. Thus, the tropical middle troposphere and especially the lower troposphere would not be favorable regions for meridional propagation to the SH extratropics.

Southern Hemisphere maps of days 10–30 summer ensemble mean z'_{200}, that is, eddy geopotential height at 200 hPa (Fig. 21), are suggestive of enhanced meridional propagation in CLDRADI's upper troposphere from the SH 12°–28°S latitude belt to the extratropics. Ignoring phase discrepancies, CLDRADI's quasi-stationary z' eddies are comparable in amplitude to the observed, whereas LONDON's are much weaker. Also,

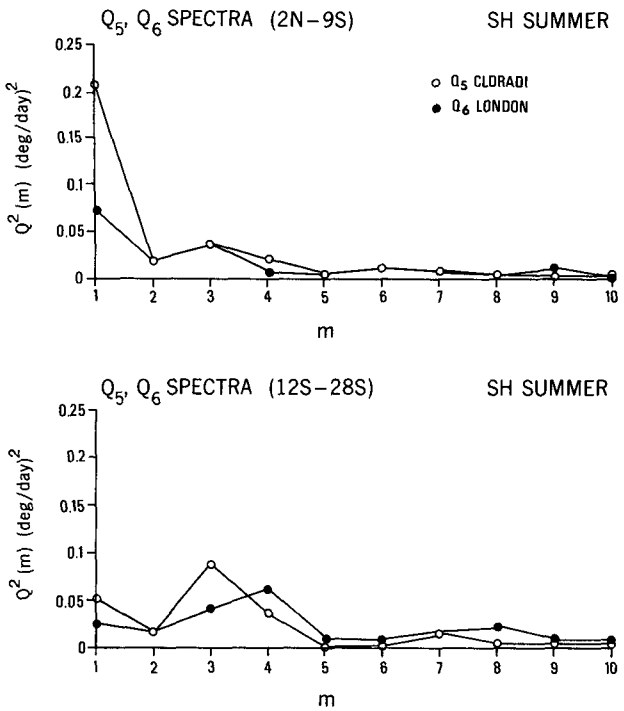

FIG. 20. Twenty-day (days 10–30) SH summer ensemble-mean, upper-tropospheric eddy total diabatic heating spectra vs zonal wavenumber for tropical latitude belts 2°N–9°S (top) and 12°–28°S (bottom). CLDRADI Q_5' and LONDON Q_6' spectra are plotted.

the orientation of the CLDRADI disturbances in the eastern Pacific and near Africa seems consistent with southward meridional propagation (Karoly, personal communication, 1989). This is not necessarily true of the LONDON and observed wave trains in the east-central Pacific, however, as they are oriented somewhat differently; and the observed wave train is more confined to the extratropics.

b. Proposed mechanism for the SH summer amplification

We speculate that in *our* GCM, the amplification of SH quasi-stationary planetary wave activity during austral summer may correspond to the excitation of a midlatitude Rossby wave train by eddy diabatic heating in the SH tropical upper troposphere. The following scenario is envisioned. Weak planetary-scale disturbances are forced in the SH tropical–subtropical upper troposphere by eddy diabatic heating. This occurs in both sets of integrations, although the eddy forcing is somewhat stronger in CLDRADI. But only CLDRADI's upper-level mean wind conditions in the tropics, *induced by cloud–radiation interaction,* are favorable for meridional energy propagation between the tropics and the SH summer extratropics. This factor may be the more critical one.

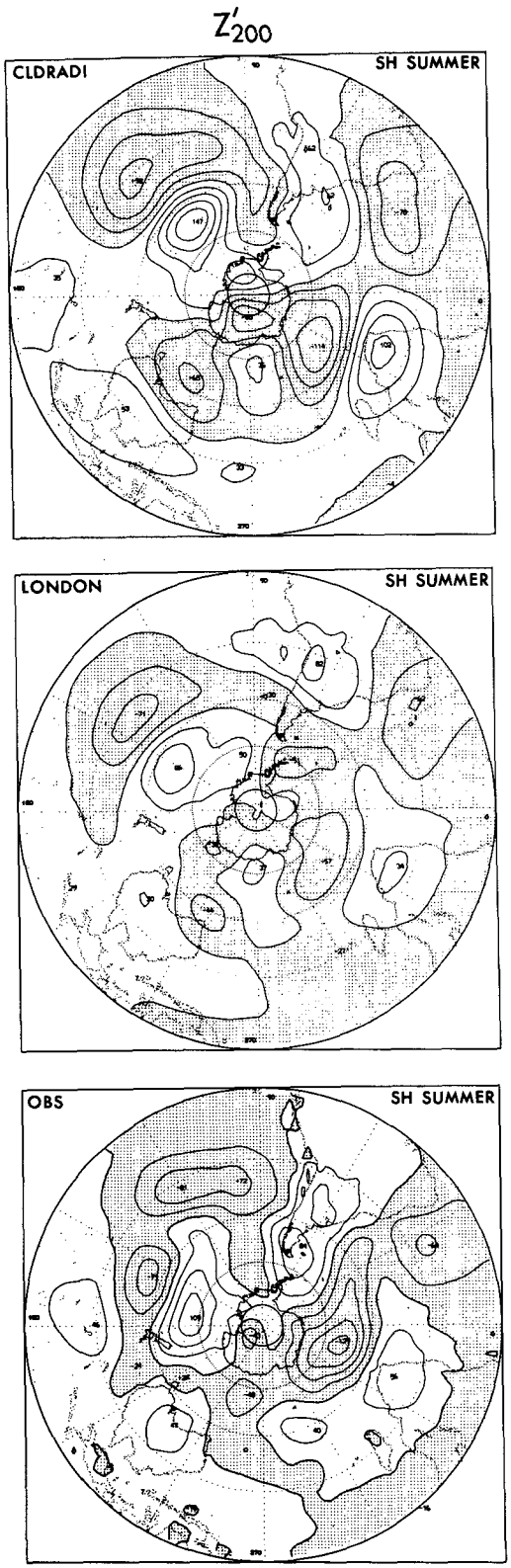

FIG. 21. Twenty-day (days 10–30) SH summer ensemble-mean z'_{200} eddy geopotential height. CLDRADI (top), LONDON (middle), NMC observations (bottom). Contour interval = 3 dam. Negative values are stippled.

Berbery and Nogués-Paegle (1992) have inferred a link between *observed* SH midlatitude eddy disturbances and OLR forcing in the 10°N–10°S equatorial belt during austral summer and have demonstrated that the mean wind conditions are more favorable for meridional propagation in the SH at that time. Intuitively, weaker in situ asymmetric forcing (land–sea thermal contrast and orography) in SH summer, as compared to the NH winter extratropics, may make the response easier to detect in the SH. Also, as suggested by Berbery and Nogués-Paegle (1992), the mechanism is probably less viable during SH winter for two reasons. First, the tropical diabatic forcing moves northward into the NH. Second, a vertical wall of zonal-mean easterlies exists in the tropics south of the ITCZ in CLDRADI, as well as LONDON and observation, thereby inhibiting meridional propagation. In addition, baroclinic growth rates of SH mid- to high-latitude disturbances might be larger during austral winter.

Among alternative mechanisms for the intensification of the SH summer extratropical quasi-stationary waves is baroclinic instability associated with CLDRADI's enhanced meridional temperature gradient at ~700 hPa and 50°S (Fig. 15) and/or at ~150 hPa and 40°S (Fig. 14). The upper-level gradient may itself be supported by CLDRADI's *zonal-mean* diabatic heating rate (~0.75 K day^{-1}) and the CLDRADI–LONDON differential diabatic heating rate (~0.5 K day^{-1}) in the 2°N–9°S tropical domain between ~156 and 223 hPa. The latter heating rates are considerably stronger than the corresponding *eddy* diabatic heating rates. But by itself, the baroclinic hypothesis may not explain the selective amplification of wavenumbers 1 and 3 or the essentially barotropic character of the CLDRADI quasi-stationary response.

Incidentally, LONDON-adj's SH summer z'_{500} field and z' spectra resemble LONDON's more than CLDRADI's. Curiously, its zonal-mean meridional temperature profile between the equator and 50°S at 700 hPa resembles CLDRADI's. Yet LONDON-adj lacks CLDRADI's stronger tropical zonal-mean and eddy diabatic heating, zonal-mean westerlies, and stronger meridional temperature gradient at ~150 hPa. Thus, whatever the precise mechanism may be, the tropical upper troposphere seems to play a role in the wave-amplification process.

10. Summary of results

A parameterization package for cloud–radiation interaction has been incorporated into a spectral GCM used for extended-range prediction studies. It consists of three basic elements: (i) cloud amount is predicted for low, middle, and high stratiform clouds as well as convective and shallow convective clouds, based on a modified version of Slingo's (1987) empirical scheme; (ii) optical depths of warm low, middle, and high clouds and precipitating high clouds, including anvil cirrus, are specified, whereas the optical depth of other subfreezing clouds varies with temperature, based upon the formulation of Harshvardhan et al. (1989); (iii) long- and shortwave cloud optical properties are linked to the cloud optical depth, following Joseph et al. (1976), as suggested by V. Ramaswamy. Also, we verified the predicted clouds and we examined the GCM's extended-range, radiative, thermal, zonal wind, and geopotential height responses by performing two sets of 30-day integrations from *real* initial conditions for three NH winter and three NH summer cases: (i) CLDRADI, with cloud–radiation interaction; and (ii) LONDON, with specified climatological zonal-mean cloud amount and global-mean cloud optical properties as the control. A few auxiliary integrations were performed, mainly to clarify some points. For some of the cases, we could compare predicted radiative fluxes directly with observed ERB data from *Nimbus-7* and ERBE satellites, or total cloud amount with observed STOWE or ISCCP data.

The geographical and zonal-mean distributions of CLDRADI total and high cloud amount bore qualitative resemblance to observation, especially in the tropics. The global-mean total cloud amount was within respectable limits, but perhaps 5% or 6% too low. The CLDRADI scheme was partially successful in detecting marine stratocumulus off the west coast of South America during SH summer, but did not predict stratocumulus off the California coast during NH summer. Also, CLDRADI predicted less total cloud cover than ISCCP over the SH circumpolar low pressure belt and Antarctica, and, to a lesser extent, over the North Pacific and North Atlantic. The cloudiness increased in the extratropics when the model's spectral resolution was refined to R42.

Among the more favorable time-mean radiative responses, the 30-day mean CLDRADI OLR fields tended to capture the gross longitudinal structure of the observed SPCZ and the ITCZ over the Pacific, despite some discrepancies in amplitude and phase. In contrast, the LONDON OLR was much more zonally symmetric in the tropics. But even the CLDRADI ITCZ fizzled out over the equatorial central Atlantic. Also, the cloud–radiation interaction scheme did not reduce the zonal-mean bias in OLR, absorbed shortwave, or net radiation fluxes. At ITCZ latitudes, the OLR biases were of $O(+10$ W m$^{-2})$ in winter and of $O(+25$ W m$^{-2})$ in summer. Negative biases in *tropical* absorbed shortwave flux suggest that CLDRADI as well as LONDON clouds are too reflective in the tropics. Conversely, both CLDRADI and LONDON exhibited a large positive bias in absorbed shortwave radiation at high latitudes of the summer hemisphere.

In the model with cloud–radiation interaction, the tropical OLR anomaly response to strong surface boundary forcing, that is, SST anomalies during the 1983 El Niño event, agreed qualitatively with observation. However, the amplitude of the response was too weak at T30L18 resolution.

A differential zonal-mean longwave radiative heating response of ~ 0.5 K day^{-1}, associated with cirrus-level clouds, was found in the tropical upper troposphere; and CLDRADI's exhibited a prominent eddy structure. Longwave heating was the dominant contributor to the net radiative heating. Approximately 75% of the radiative response in the middle-to-lower troposphere was attributed to a greater sensitivity of LONDON clouds to the radiation code's lack of explicit vertical smoothing of in-cloud longwave cooling.

The cloud optical depth increased in the tropical upper troposphere when the temperature-dependent formulation for cold (nonanvil) cirrus, based on Harshvardhan et al. (1989), was switched off. Then, the zonal-mean tropical OLR bias reversed sign and its magnitude decreased slightly, whereas the negative shortwave bias in the tropics increased. Cold and/or thin low clouds at high latitudes have insufficient optical depths.

In the tropics, the zonal-mean temperature-difference response and the acceleration of the equatorial zonal mean westerlies during NH winter seemed quite robust. The cold bias in the tropical upper troposphere decreased by ~ 1–2 K, as a consequence of (anvil) cirrus warming, though we cannot say whether the vertical profile of the radiative warming was correct. The thermal response near the LONDON low cloud tops was even stronger, mainly because CLDRADI-predicted clouds were less sensitive than the LONDON fixed clouds to the suppression of vertical smoothing of in-cloud longwave cooling profiles in the radiation code. Over Antarctica, the lower-tropospheric zonal-mean temperature bias decreased in CLDRADI in both SH summer and winter because of the reduced cloud amount, the proximity of CLDRADI low clouds to the surface, and/or thinner low cloud optical depths. Observations of the vertical distributions of cloud amount and cloud optical depth, or of radiative cooling/heating rates, could confirm whether the reduction in zonal-mean temperature biases in the tropics and over Antarctica occurred for the right reasons.

The westerly acceleration in the equatorial belt, the deceleration of the midlatitude SH westerlies, and the equatorward expansion of the NH westerly jet were prominent features of the zonal-mean zonal-wind response to cloud–radiation interaction during NH winter. Also, the minimum zonal-mean sea level pressure of the circumpolar low near latitude 60°S decreased from 998 hPa in LONDON to 993 hPa in CLDRADI, or $\sim$ by 5 hPa during SH summer. Though there were some signs of marginal improvement in the geopotential anomaly correlations in the extratropics, the very low background values of forecast skill in combination with the small sample size failed to inspire much confidence in those results.

The amplification of the quasi-stationary planetary waves in the SH summer extratropics was a rather intriguing dynamical response to cloud–radiation interaction. It resulted, perhaps, from the simultaneous existence in CLDRADI of (i) eddy diabatic forcing of planetary-scale disturbances in the SH tropical upper troposphere; and (ii) favorable mean flow conditions for meridional energy propagation to higher latitudes. LONDON also met condition (i), though CLDRADI's eddy diabatic forcing was somewhat stronger. But more crucially, only CLDRADI met condition (ii) (cf. CLDRADI's zonal mean westerlies vs LONDON's easterlies). While the response was modestly robust, more cases would be needed to establish statistical significance.

Strictly speaking, our CLDRADI–LONDON responses were obtained primarily for a particular GCM and model resolution. However, we also briefly indicated the sensitivity of the clouds to some recent improvements to the model. For example, we did not find a sharp decrease in global-mean total cloud amount in the higher resolution CLDRADI-scg R42L18 model prediction, in apparent contrast to Kiehl and Williamson (1990). In fact, in the R42 model, the predicted total cloud amount increased at high latitudes, especially over Antarctica, whereas the zonal-mean *high* cloudiness decreased moderately, that is, by $\sim 4\%$ in the ITCZ, and the zonal-mean outgoing longwave radiation correspondingly increased by only a few watts per square meter. Also, the total cloudiness decreased moderately in the subtropics, in response to improved physics. Finally, the zonal mean temperature and zonal wind responses in the tropical upper troposphere essentially held up in the CLDRADI-scg model, while the CLDRADI-scg forecast of z_{1000} improved somewhat in the extratropics due to the reformulated gravity-wave drag.

Model improvements. Parameters such as the threshold vertical motion and threshold relative humidity will be reexamined and perhaps retuned for the higher-resolution model. The optical depth of cold and/or thin low clouds at high latitudes will be increased. Also, the current assumption, that convective and stratiform clouds randomly overlap, may be modified in the radiative transfer code to treat deep convective clouds as vertically contiguous bodies. Finally, we plan to improve the model's physical description of clouds and to enhance its network of cloud–radiation interactions by incorporating cloud liquid water as a prognostic variable.

Acknowledgments. I am indebted to Drs. K. Miyakoda, V. Ramaswamy, A. Da Silva, and F. Lipps for reading the manuscript and for offering valuable suggestions. Dr. V. Ramaswamy kindly provided me with code to compute cloud optical properties from the cloud optical depth. D. Schwarzkopf helped to revise the Fels–Schwarzkopf radiative transfer code to accommodate the cloud–radiation interaction scheme and to permit efficient computation of clear-sky radiative fluxes. W. F. Stern provided initial conditions for

the integrations and some of the graphics programs. The figures were patiently drafted by P. Tunison and C. Raphael and photographed by J. Connor.

REFERENCES

Ardanuy, P. E., and H. C. Kyle, 1986: El Niño and outgoing longwave radiation: Observations from *Nimbus-7* ERB. *Mon. Wea. Rev.*, **114,** 415–433.

Barkstrom, B. R., E. F. Harrison, and R. B. Lee, III, 1990: Earth radiation budget experiment, preliminary seasonal results. *EOS,* **71,** No. 9, 297, 304–305.

Berbery, E. H., and J. Nogués-Paegle, 1992: Tropical–extratropical interactions in the Southern Hemisphere. *J. Atmos. Sci.,* **49,** submitted.

Bignell, K. J., 1970: The water-vapor infra-red continuum. *Quart. J. Roy. Meteor. Soc.,* **96,** 390–403.

CAS/JSC Working Group on Numerical Experimentation, 1988: Workshop on systematic errors in models of the atmosphere. WMO/TD No. 273, Report No. 12, December 1988. Toronto, Canada, 382 pp.

Fels, S. B., and M. D. Schwarzkopf, 1975: The simplified exchange approximation: A new method for radiative transfer calculations. *J. Atmos. Sci.,* **32,** 1476–1488.

——, and ——, 1981: An efficient, accurate algorithm for calculating CO_2 15-μm band cooling rates. *J. Geophys. Res.,* **86**(C2), 1205–1232.

Gordon, C. T., 1986: Boundary layer parameterizations and land surface processes in GFDL GCM's. *Proc. ISLSCP Conference,* Rome, Italy, ESA SP-**248,** 23–36.

——, and W. F. Stern, 1982: A description of the GFDL global spectral model. *Mon. Wea. Rev.,* **110,** 625–644.

——, and R. D. Hovanec, 1985: A simple scheme for generating two layers of radiatively constrained effective clouds in GCM's. *J. Geophys. Res.,* **90**(D6), 10 563–10 585.

Harshvardhan, D. A. Randall, T. G. Corsetti, and D. A. Dazlich, 1989: Earth radiation budget and cloudiness simulations with a general circulation model. *J. Atmos. Sci.,* **46,** 1922–1942.

Herman, G., M.-L. Wu, and W. T. Johnson, 1980: The effects of clouds on the earth's solar and infrared radiation budgets. *J. Atmos. Sci.,* **37,** 1251–1261.

Joseph, J. H., and W. J. Wiscombe, 1976: The delta-Eddington approximation for radiative flux transfer. *J. Atmos. Sci.,* **33,** 2452–2459.

Karoly, D. J., R. A. Plumb, and M. Ting, 1989: Examples of the horizontal propagation of quasi-stationary waves. *J. Atmos. Sci.,* **46,** 2802–2811.

Kiehl, J. T., and V. Ramanathan, 1990: Comparison of cloud forcing from the Earth Radiation Budget Experiment with that simulated by the NCAR Community Climate Model. *J. Geophys. Res.,* **95**(D8), 11 679–11 697.

——, and D. L. Williamson, 1990: Dependence of cloud amount on horizontal resolution in the NCAR Community Climate Model. *J. Geophys. Res.,* **96**(D6), 10 955–10 980.

Lacis, A. A., and J. E. Hansen, 1974: A parameterization for the absorption of solar radiation in the earth's atmosphere. *J. Atmos. Sci.,* **31,** 118–132.

London, J., 1957: A study of the atmospheric heat balance. Final Report, AFCRC *Contract* **AF19**(122)-165, 99 pp., N.Y. Univ. [Available from NOAA, Users Services Branch, D822, Library & Info. Services Div., 6009 Executive Blvd. WSC-4, Rockville, MD 20852.]

McClatchey, R. A., W. Fenn, J. E. A. Selby, F. E. Volz, and J. S. Garing, 1972: Optical properties of the atmosphere (3rd edition). AFCRL-72-0497, Environmental Research Papers No. 411, Air Force Cambridge Research Laboratory, L. G. Hanscom Field, Bedford, Massachusetts, 113 pp. [Available from the Defense Technical Information Center, Cameron Station, Alexandria VA, 22314. Cat. No. AD-753-075.]

Meehl, G. A., and B. A. Albrecht, 1988: Tropospheric temperatures and Southern Hemisphere circulation. *Mon. Wea. Rev.,* **116,** 953–960.

Miyakoda, K., and J. Sirutis, 1977: Comparative integrations of global models with various parameterized processes of subgrid-scale vertical transports: Description of the parameterizations. *Contrib. Atmos. Phys.,* **50,** 445–488.

——, ——, and J. Ploshay, 1986: One-month forecast experiments—without anomaly boundary forcings. *Mon. Wea. Rev.,* **114,** 2363–2401.

Platt, C. M. R., 1983: On the bispectral method for cloud parameter determination from satellite VISSR data: Separating broken cloud and semitransparent cloud. *J. Climate Appl. Meteor.,* **22,** 429–439.

——, and Harshvardhan, 1988: Temperature dependence of cirrus extinction: Implications for climate feedback. *J. Geophys. Res.,* **93** (D9), 11 051–11 058.

Pierrehumbert, R. T., 1987: An essay on the parameterization of orographic wave drag. *Proc. of the ECMWF Seminars on Orographic Effects.* Reading, England, European Centre for Medium-Range Weather Forecasts.

Ramanathan, V. E., E. J. Pitcher, R. C. Malone, and M. L. Blackmon, 1983: The response of a spectral general circulation model to refinements in radiative processes. *J. Atmos. Sci.,* **40,** 605–630.

——, R. D. Cess, E. F. Harrison, P. Minnis, B. R. Barkstrom, E. Ahmad, and D. Hartmann, 1989: Cloud-radiative forcing and climate: Results from the Earth Radiation Budget Experiment. *Science,* **243,** 57–63.

Ramaswamy, V., and V. Ramanathan, 1989: Solar absorption by cirrus clouds and the maintenance of the tropical upper troposphere thermal structure. *J. Atmos. Sci.,* **46,** 2293–2310.

Randall, D. A., Harshvardhan, D. A. Dazlich, and T. G. Corsetti, 1989: Interactions among radiation, convection, and large-scale dynamics in a general circulation model. *J. Atmos. Sci.,* **46,** 1943–1970.

Robock, A., 1980: The seasonal cycle of snow cover, sea ice and surface albedo. *Mon. Wea. Rev.,* **108,** 267–285.

Rossow, W. B., and A. A. Lacis, 1990: Global, seasonal cloud variations from satellite radiance measurements. Part II. Cloud properties and radiative effects. *J. Climate,* **3,** 1204–1253.

——, L. C. Garder, and A. A. Lacis, 1989: Global, seasonal cloud variations from satellite radiance measurements. Part I. Sensitivity of analysis. *J. Climate,* **2,** 419–458.

Sasamori, T., J. London, and D. V. Hoyt, 1972: Radiation budget of the Southern Hemisphere *Meteorology of the Southern Hemisphere.* C. W. Newton, Ed., *Meteorol. Monogr.,* **13,** Amer. Meteor. Soc., Boston, 9–23.

Schwarzkopf, M. D., and S. B. Fels, 1991: The simplified exchange method revisited: An accurate, rapid method for computation of infrared cooling rates and fluxes. *J. Geophys. Res.,* **96**(D5), 9075–9096.

Shukla, J., and Y. Sud, 1981: Effect of cloud-radiation feedback on the climate of a general circulation model. *J. Atmos. Sci.,* **38,** 2337–2353.

Sirutis, J., and K. Miyakoda, 1990: Subgrid scale physics in 1-month forecasts. Part I: Experiment with four parameterization packages. *Mon. Wea. Rev.,* **118,** 1043–1064.

Slingo, A., and J. M. Slingo, 1988: The response of a general circulation model to cloud longwave radiative forcing. I: Introduction and initial experiments. *Quart. J. Roy. Meteor. Soc.,* **114,** 1027–1062.

——, R. C. Wilderspin, and R. N. B. Smith, 1989: Effect of improved physical parameterizations on simulations of cloudiness and the earth's radiation budget. *J. Geophys. Res.,* **94**(D2), 2281–2301.

Slingo, J. M., 1987: The development and verification of a cloud prediction scheme for the ECMWF model. *Quart. J. Roy. Meteor. Soc.,* **113,** 899–927.

Smiley, V. N., B. M. Whitcomb, B. M. Morley, and J. A. Warburton, 1980: Lidar determinations of atmospheric ice crystal layers at South Pole during clear-sky precipitation. *J. Appl. Meteor.,* **19,** 1074–1090.

Smith, R. N. B., 1990: A scheme for predicting layer clouds and their water content in a general circulation model. *Quart. J. Roy. Meteor. Soc.*, **116,** 435–460.

Stephens, G. L., 1978: Radiation profiles in extended water clouds. II: Parameterization schemes. *J. Atmos. Sci.*, **35,** 2123–2132.

——, and P. J. Webster, 1981: Clouds and climate: Sensitivity of simple systems. *J. Atmos. Sci.*, **38,** 235–247.

Stern, W. F., and R. T. Pierrehumbert, 1988: The impact of an orographic gravity wave drag parameterization on extended range predictions with a GCM. Preprints, *Eighth Conf. on Numerical Weather Prediction,* Baltimore, Amer. Meteor. Soc., 745–750.

Stowe, L. L., H. Y. M. Yeh, T. F. Eck, C. G. Wellemeyer, and H. L. Kyle, 1989: *Nimbus-7* global cloud climatology. Part II: First year results. *J. Climate,* **2,** 671–709.

Sundqvist, H., 1978: A parameterization scheme for non-convective condensation including prediction of cloud water content. *Quart. J. Roy. Meteor. Soc.*, **104,** 677–690.

Telegadas, K., and J. London, 1954: A physical model of the northern hemisphere troposphere for winter and summer. Sci. Rep 1, *Contract* AF **19**(122)-165, Res. Div., Coll. Eng., N.Y. Univ. 55 pp. [Available from NOAA, User Services Branch, D822, Library & Info. Services Div., 6009 Executive Blvd. WDC-4, Rockville, MD 20852. Cat. No. M(055).N532S #1.]

Tiedtke, M., W. A. Heckley, and J. Slingo, 1988: Tropical forecasting at ECMWF: The influence of physical parameterization on the mean structure of forecasts and analyses. *Quart. J. Roy. Meteor. Soc.*, **114,** 639–664.

Ting, M.-F., and I. M. Held, 1990: The stationary wave response to a tropical SST anomaly in an idealized GCM. *J. Atmos. Sci.*, **47,** 2546–2566.

Wetherald, R. T., and S. Manabe, 1980: Cloud cover and climate sensitivity. *J. Atmos. Sci.*, **37,** 1485–1510.

Xu, K-M., and S. K. Krueger, 1991: Evaluation of cloudiness parameterizations using a cumulus ensemble model. *Mon. Wea. Rev.*, **119,** 342–367.

Zheng, Q., and L.-N. Liou, 1986: Dynamic and thermodynamic influences of the Tibetan Plateau on the atmosphere in a general circulation model. *J. Atmos. Sci.*, **43,** 1340–1354.